Analytical Studies of Wave Modes with Transverse Static Electric Fields

P. Bakshi

Physics Department, Boston College
Chestnut Hill, MA 02167

Final Technical Report

for

N00014-86-K-2016

Submitted to

Naval Research Laboratory
Washington, D.C. 20375

February 1989

I. Introduction

The ion-cyclotron instability has been of considerable interest in the study of space, as well as laboratory plasmas.[1-9] Various non-local aspects due to magnetic shear were discussed by Ganguli, Palmadesso and the present author.[5,6,8,9] A novel mechanism for the generation of electrostatic ion-cyclotron like modes was recently proposed by Ganguli, Lee and Palmadesso.[10] According to this picture, a non-uniform transverse electric field produces regions of negative and positive wave energies and a non-local wave packet can couple these domains, with a resultant transfer of energy which allows the wave mode to grow. The dispersion relation for a sharp boundary electric field had been developed which brought out the essential physical mechanism for the instability. To develop a treatment for an electric field with a smooth profile and determine the ensuing changes in the dispersion relation was one of the problems to be explored. Going beyond the second order differential equation formulation was another generalization to be considered. Also to be considered was the comparison of the above mentioned instability with the Kelvin-Helmholtz instability for the corresponding field profiles.

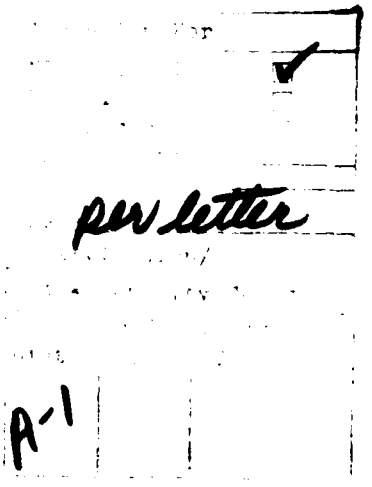

II. Accomplishments

A brief summary of the contributions made during the grant period is given below.

More realistic continuous velocity profiles $V_E(\chi,L,a)$ were considered[11] instead of the previous, piecewise continuous (top-hat) model[10]. The overall width of the velocity profile is governed by the parameter L, while the parameter a provides a continuous transition from the piecewise continuous profile (a=0), through a sequence of increasingly smoother profiles, to a Gaussian. Also considered were a trapezoid profile of overall width L and Steepness parameter a, and a generalized $\text{sech}^2(\chi/a)$ profile. The Numerov (shooting code) technique was used to solve numerically the second order differential equation to find the eigenmodes for the Ion Cyclotron (IC)-like mode.

Corresponding analysis was also carried out[11] for the trapezoid and generalized $\text{sech}^2(\chi/a)$ profiles to determine the growth rates for the Kelvin-Helmholtz (KH) instability. An analytical solution can be given for the trapezoid profile.

The main conclusions were (i) a magnetized plasma with transverse electric field is unstable to two modes, KH for long wavelengths ($k\rho_i \ll 1$) and IC for $k\rho_i > 1$; (ii) the KH mode is important when $ka<1$, and dominates for steeper profiles; (iii) the new mode (IC) has a relatively weak dependence on 'a' but depends strongly on L. For smooth profiles ($\text{sech}^2(\chi/a)$) the peak of the growth rate for IC is comparable to the KH growth rate, and the two instability bands are widely separated in R-space. This mode should thus be observable in simulations or experiments; (iv) since a sharp profile quickly relaxes to a smoother profile (increase in a), the IC type mode becomes dominant after the

initial transient dynamics.

These results were presented at the AGU Meeting, December 1986 (Ref. 11, copy of Abstract is attached.)

We have also considered the generalizations needed to go beyond the second order differential equation descriptions. Explicit dispersion equations were obtained for the 4th and 6th order differential equations level of description. Also, all of these are successive approximations to a full integral equation treatment. A full kinetic theory integral equation treatment was provided in Ref. 12. Formal reduction leads to the differential equation descriptions for the KH modes for $k\rho_i \ll 1$ and the IC-like modes for $k\rho_i \gg 1$. (Copy of Ref. 12 is attached.)

III. References

1. W.E. Drummond and M.N. Rosenbluth, Phys. Fluids 5, 1507 (1962).

2. M.C. Kelley, E.A. Bering, and F.S. Mozer, Phys. Fluids 18, 1590 (1975). E. Ungstrup, D.M. Klumpar, and W.J. Heikkila. J. Geophys. Res., 84, 4289 (1979); R.W. Fredericks and C.T. Russel, J. Geophys. Res., 78, 2917 (1973); K. Papadopoulos, Rev. Geophys. Space. Phys. 15,113 (1977).

3. N.D. D'Angelo and R.W. Motely, Phys. Fluids 5, 633 (1962); R.W. Motely and N.D. D'Angelo, Phys. Fluids 6, 296 (1963).

4. J.M. Kindel and C.F. Kennel, J. Geophys. Res. 76, 3055, (1971).

5. G. Ganguli and P. Bakshi, Phys. Fluids, 25, 1830, (1982).

6. P. Bakshi, G. Ganguli and P. Palmadesso, Phys. Fluids, 26, 1808, (1983).

7. R. Schrittwieser, Phys. Fluids, 26, 2250 (1983); S.L. Cartier, N. D'Angelo, P.H. Drumm and R.L. Merlino, Phys. Fluids, 28, 432 (1983); G. Popa, J. Juul Rasmussen and R. Schrittwieser, Phys. Lett. A, (to appear).

8. G. Ganguli, P. Bakshi and P. Palmadesso, J. Geophys. Res., 89, 945, (1984).

9. G. Ganguli, P. Bakshi and P. Palmadesso, Phys. Fluids, 27, 2039, (1984).

10. G. Ganguli, Y.C. Lee and P. Palmadesso, Phys. Fluids, 28, 761, (1985).

11. G. Ganguli, P. Bakshi and P. Palmadesso, "High Frequency Instability in a Magnetoplasma for Various Transverse Electric Field Profiles", Transactions of AGU, EOS, 67, 1168 (1986).

12. G. Ganguli, Y.C. Lee and P. Palmadesso, "Kinetic Theory for Electrostatic Waves due to Transverse Electric Fields", Phys. Fluids, 31, 823 (1988).

EOS, Vol. 67, P. 1168, (1986).

(Transactions, American Geophysical Union).

SM32B-9M 1330H POSTER

High Frequency Instability in a Magnetoplasma for Various Transverse Electric Field Profiles*

C. GANGULI (Science Applications International Corp., McLean, VA 22012)
P. BAKSHI (Boston College, Chestnut Hill, MA 02167)
P. PALMADESSO (Naval Research Laboratory, Washington, DC 20375)

A new instability mechanism[1] giving rise to high frequency short wavelength oscillations in a magnetoplasma with transverse electric field was recently proposed. That study was based on an idealized (piecewise constant) velocity profile. We consider more realistic profiles $V_E(x,L,a)$, where variation of the parameter a provides a continuous transition from the piecewise constant profile through a sequence of increasingly smoother profiles, and finally to a Gaussian. The overall width is governed by the parameter L. We find that the growth rate is relatively insensitive to the variation of the steepness parameter a, but has a stronger dependence on the extent L. This conclusion is also borne out for other profiles as well. We also compare the growth rates for the fluid Kelvin-Helmholtz instability with our results (considering a trapezoid profile[2]) and note that, as may be expected, the Kelvin-Helmholtz mode is important for the long wavelength domain[3], while the new instability is significant for the shorter wavelengths. In fact, for a wide range of parameters, the two instability bands are quite distinct on the growth rate versus wavelength plot. Various scalings with physical parameters are discussed.

* Work supported by ONR and NASA.

1. Ganguli, G., Y.C. Lee, and P. Palmadesso, Phys. Fluids, 28, 761, 1985.
2. Drazin, P.G. and L.N. Howard, J. Fluid Mech., 9, 257, 1962.
3. A recent study by Fritchett, UCLA report #PPG 878 (1985) shows that the fluid growth rates of the Kelvin-Helmholtz modes are further reduced by taking into account the finite Larmor radius corrections.

Kinetic theory for electrostatic waves due to transverse velocity shears

G. Ganguli and Y. C. Lee[a)]
Science Applications International Corporation, 1710 Goodridge Drive, McLean, Virginia 22012
P. J. Palmadesso
Plasma Physics Division, Naval Research Laboratory, Washington, D.C. 20375-5000

(Received 29 July 1987; accepted 3 December 1987)

A kinetic theory in the form of an integral equation is provided to study the electrostatic oscillations in a collisionless plasma immersed in a uniform magnetic field and a nonuniform transverse electric field. In the low temperature limit ($k_y\rho_i \ll 1$, where k_y is the wave vector in the y direction and ρ_i is the ion gyroradius) the dispersion differential equation is recovered for the transverse Kelvin–Helmholtz modes for arbitrary values of $k_\parallel$, where $k_\parallel$ is the component of the wave vector in the direction of the external magnetic field assumed in the z direction. For higher temperatures ($k_y\rho_i > 1$) the ion-cyclotron-like modes described earlier in the literature by Ganguli, Lee, and Palmadesso [Phys. Fluids **28**, 761 (1985)] are recovered. In this article the integral equation is reduced to a second-order differential equation and a study is made of the kinetic Kelvin–Helmholtz and the ion-cyclotron-like modes that constitute the two branches of oscillation in a magnetized plasma including a transverse inhomogeneous ac electric field.

I. INTRODUCTION

Shear in the flow velocity of a fluid leads to the low frequency and long wavelength Kelvin–Helmholtz (KH) instability.[1] The velocity shear can be generated in a number of ways. In a plasma the existence of an inhomogeneous electric field component transverse to the ambient uniform magnetic field can provide a transverse velocity shear. The evolution of the KH instability in this configuration has been extensively studied.[2]

Recently some space observations[3] and laboratory experiments[4] seem to indicate that ion-cyclotron-like waves are observed for subcritical field aligned currents and therefore the origin of these waves is somewhat mysterious. A crucial feature of these observations and experiments was the presence of a transverse component of a zeroth-order electric field. In order to study the role of the transverse electric fields in the generation of the ion-cyclotron-like waves[3,4] we suggested a mechanism based on the coupling of the negative energy ion Bernstein modes (or the ion-cyclotron modes) in the region where the dc electric field is localized, with the positive energy ion Bernstein modes (or the cyclotron modes) in the region where the dc electric field is absent.[5] This is similar to the negative energy wave growth in an inhomogeneous mirror geometry.[6] In our initial theory we idealized a typical electric field profile by a piecewise continuous function for simplicity. The gradients of the electric field were ignored to avoid the KH modes for which the second derivative of the electric field is necessary. Here we use kinetic theory to obtain the general dispersion relation rigorously, for the electrostatic oscillations in a plasma, in the form of an integral equation for an arbitrary electric profile. In various limits we reduce the integral equation to second-order differential equations to obtain the eigenvalues. The integral equation will be solved in a subsequent paper.

[a)] Permanent address: University of Maryland, College Park, Maryland 20742.

II. THEORY

The equation of motion of a charged particle in a uniform magnetic field in the z direction and a nonuniform electric field in the x direction is given by

$$\frac{d^2}{dt^2}\mathbf{r} = \frac{e}{m}E(x)\hat{x} + \Omega \mathbf{v}\times\hat{z}, \tag{1}$$

where $\Omega = eB_0/mc$ is the gyrofrequency, and e, m, and B_0 are the charge, mass, and the ambient uniform magnetic field, respectively. The constants of the motion are (i) $H = (v_x^2 + v_y^2 + v_z^2)/2 + e\Psi(x)/m$, the total energy, where $E(x) = -\partial\Psi(x)/\partial x$; and (ii) $X_g = x + v_y/\Omega$, which is obtained by integrating the y component of (1). Using $v_y = \Omega(X_g - x)$ in the expression for H we obtain the Hamiltonian for an equivalent one-dimensional problem:

$$H = v_x^2/2 + \Omega^2(X_g - x)^2/2 + (e/m)\Psi(x). \tag{2}$$

Minimizing the potential of (2) we obtain the guiding center position

$$\xi = x + [v_y - V_E(\xi)]/\Omega, \tag{3}$$

another constant of the motion that is an implicit function of X_g and therefore is not an independent constant of motion. Here $V_E(\xi) = -cE(\xi)/B_0$.

In order to recover the fluid KH modes as the fluid limit of the kinetic formalism, we will need to construct an equilibrium distribution function using the constants of motion, such that the equilibrium density is uniform or nearly so. However, we would also like to be able to study the more general case of an equilibrium with an arbitrary density profile. Therefore, we will choose the distribution function to be of the form $f_0(\xi,H) = n_0(\xi)F_0(\xi,H)$, such that $\int F_0\, d^3v \simeq$ const. Then we obtain an appropriate f_0 for the study of the classical KH mode by setting $n_0(\xi) =$ const, and an appropriate f_0 for the general case by relaxing this condition. Such a distribution function, which leads to an equilibrium density uniform to $O(\epsilon)$ for a constant n_0, where $\epsilon (= \rho_i/L)$ is the smallness parameter, $\rho_i (= v_{ti}/\Omega_i)$ is the

 0031-9171/88/040823-16$01.90

ion gyroradius, and L is the characteristic length associated with the external electric field, can be found by a systematic procedure and is given by

$$f_0(\xi,H) = N\exp(-\beta H)g(\xi), \tag{4}$$

where $N = n_0(\beta/2\pi)^{3/2}, \beta = 1/v_t^2, v_t$ is the thermal velocity, and

$$g(\xi) = \exp\{\beta\,[e\Psi(\xi)/m + V_E^2(\xi)/2]\}\eta(\xi)^{-1/2},$$

where $\eta(\xi) = 1 + V_E'(\xi)/\Omega$. The quantity η parametrizes the magnitude of the velocity shear. Note that there are two crucial parameters in this problem: (i) η and (ii) ϵ. We will allow η to be arbitrary but positive while assuming $\epsilon \ll 1$. The equilibrium distribution can be expressed as

$$f_0(\xi,H) = N\exp[-(\beta/2)w_1^2] \times \exp[-(\beta/2)v_z^2]/\sqrt{\eta(\xi)}, \tag{5}$$

where we have expanded the x dependence of (4) around ξ and neglected terms of $O(\epsilon^3)$ and higher. Here, w_1^2 is

$$w_1^2 = v_x^2 + \eta(\xi)u_y^2 + [V_E''(\xi)/\Omega^2](u_y\langle u_y^2\rangle - u_y^3/3), \tag{6}$$

where $u_y = v_y - \langle v_y\rangle$ and $\langle\ \rangle$ indicates the time average. It should be noted that the simplified zeroth-order state as provided in Eq. 5, has a pathological behavior when u becomes very large. In our calculations we use the transformed coordinates w_1 and Φ (see Appendix B) so that the simplified zeroth-order state as given in (5) agrees with the exact zeroth-order state as given in (4) to order ϵ^2 but which does not have this pathological property.

Integrating (5) over all velocities we can show that the equilibrium density distribution, $n = n_0[1 + o(\epsilon^2)]$, is uniform to order ϵ. It is possible to devise a distribution function with density uniform to any desired higher order in ϵ, but this is not necessary here. For generality, in the following we shall consider a nonuniform equilibrium density profile, i.e., $n_0 = n_0(\xi)$.

Now using the definitions

$$\phi(r',t') = \exp[-i(\omega t' - k_y y')]\phi(x'), \tag{7a}$$

$$\phi(x') = \int dk_x'\exp(ik_x'x')\phi_k(k_x'), \tag{7b}$$

where ϕ is the electrostatic potential for the perturbed electric field and linearizing the Vlasov equation, we obtain the perturbed distribution function

$$f_1(x,v) = -\beta\frac{e}{m}f_0\Big(\int dk_x'\exp[i(k_x'x)]\phi_k(k_x') + i\int dk_x'\,\phi_k(k_x')(\omega - k_y V_g)\int_{-\infty}^{t} dt'\,A\Big), \tag{8}$$

where $\tau = t' - t$,

$$A(t',x',y',z') = \exp\{i[k_x'x' + k_y(y'-y) + k_z(z'-z) - \omega\tau]\}, \tag{9}$$

$$V_g(\xi) = \frac{1}{\beta\eta(\xi)f_0\Omega}\frac{\partial f_0}{\partial\xi} = V_E(\xi) - \frac{V_E''(\xi)\rho^2}{2\eta^2} + \frac{\epsilon_n\rho\Omega}{\eta}. \tag{10}$$

Here, $\epsilon_n = \rho/L_n$ and $L_n = \{[dn_0(\xi)/d\xi]/n_0(\xi)\}^{-1}$ is the scale length associated with the equilibrium density profile. In order to evaluate the time integral in (8) we need the orbits. The x component of (1) gives the net force in this direction. Since v_x is oscillatory in equilibrium, $\langle\dot v_x\rangle = 0$. This leads to the expression for an average equilibrium drift $\langle v_y\rangle = \langle V_E(x)\rangle$ in the y direction. Now expanding V_E around ξ we obtain

$$\langle v_y\rangle = V_E(\xi) + \frac{V_E''(\xi)}{2\Omega^2\eta(\xi)}\langle[v_y - V_E(\xi)]^2\rangle + O(\epsilon^3). \tag{11}$$

Transforming the equation of motion (1) into a frame moving with $\langle v_y\rangle$ in the y direction (i.e., $v_y \to u_y = v_y - \langle v_y\rangle$) and to the spatial coordinate ξ (i.e., $x \to \xi$) we obtain the transformed equations of motion,

$$\dot v_x = \Omega\eta(\xi)u_y + [V_E''(\xi)/2\Omega](\langle u_y^2\rangle - u_y^2), \tag{12}$$

$$\dot u_y = -\Omega v_x,$$

where we have neglected terms of $O(\epsilon^3)$ and higher. These equations lead to (see Appendix A)

$$v_x = w_1\sin\Phi - (\hat w/6\eta^{3/2})\sin 2\Phi, \tag{13a}$$

$$u_y = (w_1/\sqrt{\eta})\cos\Phi - (\hat w/12\eta^2)\cos 2\Phi, \tag{13b}$$

and

$$x' - x = -(w_1/\sqrt{\eta}\Omega)[\cos(\sqrt{\eta}\Omega\tau + \Phi) - \cos\Phi] + (\hat w/12\eta^2\Omega)\{\cos[2(\Phi + \sqrt{\eta}\Omega\tau)] - \cos 2\Phi\}, \tag{14a}$$

$$y' - y = (w_1/\eta\Omega)[\sin(\Phi + \sqrt{\eta}\Omega\tau) - \sin\Phi] - (\hat w/24\eta^{5/2}\Omega)\{\sin[2(\Phi + \sqrt{\eta}\Omega\tau)] - \sin 2\Phi\} + \langle v_y\rangle\tau, \tag{14b}$$

$$z' - z = v_z\tau, \tag{14c}$$

where

$$w_1^2 = v_x^2 + \eta(\xi)u_y^2 + V_E''(\xi)(\langle u_y^2\rangle u_y - u_y^3/3)/\Omega^2,$$

and

$$\hat w = V_E''(\xi)w_1^2/\Omega^2.$$

Also $\Phi = \sqrt{\eta}\Omega t + \bar\Phi$, where $\bar\Phi$ is the velocity space angle at $t = 0$. The oscillatory terms of the order $\hat w$ in the orbits are not important except in the derivation of the Jacobian of transformation from the integration variables (x,v_x,v_y) to (ξ,w_1,Φ), which will be necessary in the following. For simplicity, therefore, we shall ignore the oscillatory terms of $O(\hat w)$ everywhere except in the derivation of the Jacobian. This restriction can easily be relaxed.

Using (13) and (14) in (8) we obtain

$$f_1(x,\mathbf{v}) = -\beta\frac{e}{m}f_0(\xi,H)\Bigg(\int dk_x' \exp(ik_x'x)\phi_k(k_x') - \int dk_x' \phi_k(k_x')\sum_{n'}\frac{J_{n'}(\sigma')(\omega - k_y V_g)\exp\{i[n'(\Phi-\alpha') + k_x'\bar{\xi} - (k_y w_\perp/\eta\Omega)\sin\Phi]\}}{(\omega - \sqrt{\eta}n'\Omega - k_y\langle v_y\rangle - k_z v_z)}\Bigg), \tag{15}$$

where

$$\sigma' = k_\perp' w_\perp/\Omega, \quad k_\perp'^2 = k_x'^2/\eta + k_y^2/\eta^2, \quad \alpha' = \tan^{-1}(k_x'\sqrt{\eta}/k_y), \quad \bar{\xi} = x + u_y/\Omega,$$

and $J_{n'}$ are Bessel functions. The projection of (15) in k_x is

$$f_{1k_x}(\mathbf{v}) = -\frac{\beta e}{2\pi m}\int dk_x' \phi_k(k_x')\int dx f_0 \times\Bigg(\exp[-i(k_x - k_x')x] - \sum_{n'n}\frac{J_{n'}(\sigma')J_n(\sigma)(\omega - k_y V_g)}{\omega - \sqrt{\eta}n'\Omega - k_y\langle v_y\rangle - k_z v_z} \times\exp\{i[(k_x' - k_x)\bar{\xi} + (n'-n)\Phi + n\alpha - n'\alpha']\}\Bigg) \tag{16}$$

The perturbed density is then obtained by integrating the perturbed distribution function over all velocities

$$n_{1k_x} = -\frac{\beta e}{2\pi m}\int dv_x\, dv_y\, dv_z \int dx \int dk_x' \phi_k(k_x') f_0 \times\{\exp[i(k_x' - k_x)x] - \exp[i(k_x' - k_x)\bar{\xi}]F\}, \tag{17}$$

where

$$F = (\omega - k_y V_g)\sum_{n',n}\frac{J_{n'}(\sigma')J_n(\sigma)}{\omega - n'\sqrt{\eta}\Omega - k_y\langle v_y\rangle - k_z v_z} \times\exp[i(n'-n)\Phi + in\alpha - in'\alpha']. \tag{18}$$

Equation (17) is the most general form for the perturbed density for either ions or electrons. In the quasineutral limit the most general dispersion relation for the electrostatic waves, in the form of an integral equation, is given by $\Sigma_\alpha \int \exp(ik_x x) n_{1k}^\alpha\, dk_x = 0$, where α represents the species.

Now we transform the integration variables in (17) from (x,v_x,v_y) to $(\xi,w_\perp,\Phi)$ using the appropriate Jacobian, which in this case is (see Appendix B) $|J| = -\sqrt{\eta}w_\perp$; expand the exponentials in x and $\bar{\xi}$ around ξ; and retain terms up to $O(\epsilon^2)$ to obtain

$$n_{1k_x} = -\frac{Ne\beta}{m}\int_{-\infty}^{+\infty} d\xi \int_{-\infty}^{+\infty} dv_z \int_0^\infty dw_\perp \int_0^{2\pi} d\Phi\sqrt{\eta}w_\perp \times\int_{-\infty}^{+\infty} dk_x' \phi_k(k_x')\frac{\exp[-\beta(w_\perp^2 + v_z^2)/2]}{\sqrt{\eta}} \times\exp[i(k_x' - k_x)\xi]G, \tag{19}$$

where

$$G = (1-F)\Bigg(1 - i(k_x' - k_x)\frac{V_E''(\xi)w_\perp^2}{4\eta^2\Omega^3}\Bigg) - i(k_x' - k_x)\frac{w_\perp\cos\Phi}{\eta\Omega} - (k_x' - k_x)^2\frac{w_\perp^2\cos^2\Phi}{2\eta\Omega^2}. \tag{20}$$

We shall first obtain the differential equation for the fluid KH modes as the fluid limit of (19).

A. Low temperature but arbitrary shear

Consider $k_\parallel = 0$ and $\epsilon_n = 0$. For a quasineutral plasma the condition that the net perturbed density (19) vanishes provides the electrostatic dispersion relation. Further, since $k_\parallel = 0$ the electron contribution to the net perturbed density is ignorable so that the ion perturbed density set equal to zero leads to the desired general dispersion relation. We shall now proceed to specialize the general dispersion relation for low temperature ($k_y\rho_i \to 0$). Upon Φ integration the term proportional to $\cos\Phi$ in G vanishes and n' becomes n in (18). Since low temperatures are of interest we keep $n = 0, \pm 1$ terms in F. Higher harmonics are associated with higher orders in temperature. The argument of the Bessel functions can be written as $\sigma = (w_\perp/v_t)(k_\perp L)\epsilon$ and, assuming that the factors $(k_\perp L)$ and $(w_\perp/v_t)$ are less than or of order unity, we can expand the Bessel functions to $O(\epsilon^2)$ so that

$$1 - F = 1 - \Bigg[1 + \frac{k_y(\langle v_y\rangle - V_g)}{\omega_1} - \frac{k_y^2 w_\perp^2}{2\eta^2\Omega^2}\left(1 - \frac{\omega_1^2}{\omega_1^2 - \eta\Omega^2}\right) - \frac{w_\perp^2}{4\eta\Omega^2}\Bigg(k_x'^2 + k_z^2 - \frac{2\omega_1^2 k_x k_x'}{\omega_1^2 - \eta\Omega^2} + \frac{2ik_y\omega_1\Omega(k_x' - k_x)}{\omega_1^2 - \eta\Omega^2}\Bigg)\Bigg]. \tag{21}$$

It is important to note that under these conditions the terms of order unity in $(1 - F)$ drop out. Therefore, the term proportional to $\langle v_y\rangle - V_g = V_E''(w_\perp^2/2\Omega^2 + \rho_i^2)/2\eta^2 \sim O(\epsilon^2)$, which is responsible for the KH instability, along with the other terms of the same order, are the leading terms of (19). This will lead to the dispersion differential equation (22), describing the KH modes. However, when $\sigma \sim O(1)$, the Bessel functions can no longer be expanded and consequently the role of the $O(\epsilon^2)$ terms, and in particular the V_E'' term, will diminish in importance. This situation, which corre-

sponds to cases in which $k_y\rho_i \gtrsim O(1)$ (ϵ may still be small), may lead to a significant change in the character of the mode, and possibly to finite gyroradius stabilization of the KH instability.

In order to obtain the dispersion differential equation for the KH modes we need to obtain $n_1(x) = \int n_{1k_x} \times \exp(ik_x x)dk_x$ for the ions and set it equal to zero. After carrying out the ω_1 integration, ρ_i^2 can be factored out and the resulting equation becomes temperature independent in the $\rho_i \to 0$ limit. The k_x integration provides a delta function, $2\pi\delta(x-\xi)$, which makes the ξ integration trivial and converts the ξ dependence into x dependence. Thus, performing the ξ integration after using $\int dk_x' \phi_k(k_x')\exp(ik_x'\xi) = \phi(\xi)$, we obtain the second-order differential equation for the KH modes in the zero temperature limit:

$$\left(\frac{d^2}{dx^2} - A(x)\frac{d}{dx} - B(x)k_y^2 - \frac{k_y V_E''(x)}{\omega_1} C(x)\right)\phi(x) = 0, \tag{22}$$

where

$$A(x) = [2k_y V_E'(x)\omega_1 + \eta'(x)\Omega^2]/[\omega_1^2 - \eta(x)\Omega^2], \tag{23}$$

$$B(x) = 1 + \{2[\eta(x) - 1]\Omega^2\}/[\omega_1^2 - \eta(x)\Omega^2], \tag{24}$$

$$C(x) = \Omega^2/[\omega_1^2 - \eta(x)\Omega^2], \tag{25}$$

and $\omega_1 = \omega - k_y V_E(x)$. Equation (22) is the dispersion differential equation for the fluid KH modes valid for arbitrary shear strength, i.e., for arbitrary values of V_E'/Ω_i as long as $\eta > 0$. Starting from the fluid equations one can also derive (22). It should be noted, however, that when η becomes small, the arguments of the Bessel functions become large. Thus for $\eta \to 0$ the expansion of the Bessel functions for small argument may not be a good approximation unless the ion temperatures and hence ρ_i also become vanishingly small. Thus if η is considered arbitrary then the fluid theory is valid only when $\eta > 0$ and the arguments of the Bessel functions are sufficiently small.

Pritchett and Coroniti[7] used the fluid theory to obtain the dispersion equation for the KH modes for warm plasmas. They incorporated the temperature effects through the pressure tensor and arrived at Eq. (16) of Ref. 7 as the dispersion differential equation. If the temperature related terms (which are included in the factor R in their paper) are set equal to zero in Eq. (16) of their paper,[7] then it reduces to our Eq. (22). At this stage, by defining a transformation $U = (\omega_1\phi' - k_y\Omega\phi)/D$, where $D = \eta - (\omega_1/\Omega)^2$, it can be shown that all the η related terms can be transformed away and (22) can be expressed in the form of (34), which represents the classical KH mode except that $\phi(x)$ is replaced by U. Thus, although the eigenfunctions are affected, the eigenvalues of the classical KH modes remain unaffected by the magnitude of the velocity shear in the zero temperature limit. This is physically satisfying, since if the gyroradius is zero and in the absence of an equilibrium x drift, particles cannot sample the x direction and hence cannot experience the velocity shear irrespective of its magnitude. However, for finite temperatures, the magnitude of the velocity shear will play a role, as evidenced in the simulation results[7] and the experimental results of Jassby.[8] Unfortunately in the simple model for the temperature assumed in Ref. 7 this cannot be explained since all the temperature related terms can also be transformed away.[7] For arbitrary shears the temperature correction to the lowest order involves a great many terms and will be discussed in a subsequent paper. Here we make the weak shear approximation but treat temperature as arbitrary and find that the finite gyroradius stabilization of the KH modes can be understood and predicted by the kinetic theory.

B. Weak shear but arbitrary temperature

Now we consider the limit where the shear is not strong but temperature and $k_\parallel$ are arbitrary. In this limit, since the x dependence of the equilibrium quantities is weak, we can assume $k_x \simeq k_x'$ in (20) so that $G = 1 - F$. Also for weak shears, $\eta \sim 1$ will be considered. For generality we will also include an equilibrium density profile $N(\xi)$. The perturbed density after carrying out the Φ integration becomes

$$n_{1\alpha}(x) = -\frac{e_\alpha\beta_\alpha}{m_\alpha}\int_{-\infty}^{+\infty} dk_x \exp(ik_x x)\int_{-\infty}^{+\infty} d\xi \int_0^{+\infty} dw_\perp\, w_\perp \int_{-\infty}^{+\infty} dv_z \int_{-\infty}^{+\infty} dk_x' \phi_k(k_x')N_\alpha(\xi)\exp[i(k_x' - k_x)\xi] \times \exp\left(-\frac{\beta}{2}(w_\perp^2 + v_z^2)\right)\left(1 - \sum_n \frac{(\omega_1 + \omega_{2\alpha} - \omega_\alpha^*)J_n^2(\sigma_\alpha)}{\omega_1 - \omega_{2\alpha} - n\Omega_\alpha - k_z v_z}\right). \tag{26}$$

Here α denotes the species and $\omega - k_y V_{g\alpha} = \omega_1 + \omega_{2\alpha} - \omega_\alpha^*$, where $\omega_{2\alpha} = k_y V_E'' \rho_\alpha^2/2$ and $\omega_\alpha^* = k_y \epsilon_{n\alpha}\rho_\alpha\Omega_\alpha$. In the denominator we have approximated $\omega - k_y\langle v_y\rangle \simeq \omega_1 - \omega_2$, thereby replacing $w_\perp^2$ by its average value $2v_{t\alpha}^2$. Now the $w_\perp$ and the v_z integrations can easily be performed to yield

$$n_{1\alpha}(x) = -\frac{e_\alpha\beta_\alpha}{2\pi m_\alpha}\int_{-\infty}^{+\infty} dk_x \exp(ik_x x)\int_{-\infty}^{+\infty} d\xi\, n_0(\xi)\int_{-\infty}^{+\infty} dk_x' \phi_k(k_x')\exp[i(k_x' - k_x)\xi] \times\left[1 + \sum_n\left(\frac{\omega_1 + \omega_{2\alpha} - \omega_\alpha^*}{\sqrt{2}|k_\parallel|v_{t\alpha}}\right)Z\left(\frac{\omega_1 - \omega_{2\alpha} - n\Omega_\alpha}{\sqrt{2}|k_\parallel|v_{t\alpha}}\right)\Gamma_n(b_{1\alpha})\right], \tag{27}$$

where $\Gamma_n(b) = I_n(b)\exp(-b)$, and I_n are the modified Bessel functions and $Z(\xi)$ are the plasma dispersion functions. Here $b_1 = \rho_\alpha^2(k_x^2 + k_y^2)$. We can expand Γ_n in $k_x^2\rho_\alpha^2$ so that $\Gamma_n(b_1) \sim \Gamma_n(b) + \Gamma_n'(b)k_x^2\rho_\alpha^2 + \cdots$, where $\Gamma_n' = d\Gamma_n/db$ and

$b = k_y^2 \rho_\alpha^2$. Since we have consistently retained terms up to ϵ^2, we neglect the terms $O(k_y^4 \rho_\alpha^4)$ and higher that are of higher order in ϵ. Using this expansion for $\Gamma_n(b_1)$ in (27) we perform the remaining integrals to obtain

$$n_{1\alpha}(x) = -\frac{1}{4\pi\lambda_\alpha^2 e_\alpha}\left[-\sum_n\left(\frac{\omega_1+\omega_{2\alpha}-\omega^*}{\sqrt{2}|k_\parallel|v_{t\alpha}}\right)Z\left(\frac{\omega_1-\omega_{2\alpha}-n\Omega_\alpha}{\sqrt{2}|k_\parallel|v_{t\alpha}}\right)\rho_\alpha^2\Gamma_n'(b_\alpha)\frac{d^2}{dx^2}+1\right.$$
$$\left.+\sum_n\left(\frac{\omega_1+\omega_{2\alpha}-\omega_\alpha^*}{\sqrt{2}|k_\parallel|v_{t\alpha}}\right)Z\left(\frac{\omega_1-\omega_{2\alpha}-n\Omega_\alpha}{\sqrt{2}|k_\parallel|v_{t\alpha}}\right)\Gamma_n(b_\alpha)\right]\phi(x), \tag{28}$$

where $\lambda_\alpha^2 = m_\alpha v_{t\alpha}^2/4\pi n_{0\alpha}e_\alpha^2$, is the Debye length for the species α. The quasineutrality condition, $|e|(n_{1i}-n_{1e}) = 0$, leads to the general dispersion differential equation for the electrostatic modes in the low shear limit. Retaining only the $n=0$ term for the electrons and considering $\rho_e^2 \ll \rho_i^2$ we obtain

$$\left(\rho_i^2 A(x)\frac{d^2}{dx^2}+Q(x)\right)\phi(x)=0, \tag{29}$$

where

$$A(x) = -\sum_n\left(\frac{\omega_1+\omega_2-\omega^*}{\sqrt{2}|k_\parallel|v_i}\right)$$
$$\times Z\left(\frac{\omega_1-\omega_2-n\Omega_i}{\sqrt{2}|k_\parallel|v_i}\right)\Gamma_n'(b), \tag{30}$$

and

$$Q(x) = 1+\sum_n\left(\frac{\omega_1+\omega_2-\omega^*}{\sqrt{2}|k_\parallel|v_i}\right)$$
$$\times Z\left(\frac{\omega_1-\omega_2-n\Omega_i}{\sqrt{2}|k_\parallel|v_i}\right)\Gamma_n(b)$$
$$+\tau\left[1+\left(\frac{\omega_1+\omega_2/\tau\mu+\omega^*/\tau}{\sqrt{2}|k_\parallel|v_e}\right)\right.$$
$$\left.\times Z\left(\frac{\omega_1-\omega_2/\tau\mu}{\sqrt{2}|k_\parallel|v_e}\right)\right]. \tag{31}$$

Here $\tau = T_i/T_e$, $\mu = m_i/m_e$, and $b = (k_y\rho_i)^2$. The subscripts on ω_2 and ω^*, which are for the ions, are suppressed.

In order to recover the dispersion differential equation for the KH modes in the weak shear limit we set $\omega^* = 0$, $k_\parallel = 0$, and retain $n = 0, \pm 1$ in (30) and (31) so that

$$A(x) = \left(\frac{\omega_1+\omega_2}{\omega_1-\omega_2}\right)\Gamma_0'(b)+\left(\frac{\omega_1^2-\omega_2^2}{(\omega_1-\omega_2)^2-\Omega_i^2}\right)2\Gamma_1'(b), \tag{32}$$

and

$$Q(x) = 1-\left[\left(\frac{\omega_1+\omega_2}{\omega_1-\omega_2}\right)\Gamma_0(b)\right.$$
$$\left.+\left(\frac{\omega_1^2-\omega_2^2}{(\omega_1-\omega_2)^2-\Omega_i^2}\right)2\Gamma_1(b)\right]. \tag{33}$$

Further, if we take the low temperature limit $(k_y\rho_i \ll 1$, and thus $\Gamma_0 \sim (1-b)$, $\Gamma_1 \sim b/2$, $\Gamma_0' \sim -1$, $\Gamma_1' \sim \frac{1}{2}]$ and the low frequency limit $(\omega_1^2/\Omega_i^2 \ll 1)$ in (32) and (33) and substitute these in (29), we recover the starting differential equation for the KH modes widely used in the literature[5]:

$$\left(\rho_i^2\frac{d^2}{dx^2}-k_y^2\rho_i^2+\frac{k_y V_E''(x)}{\omega_1}\rho_i^2\right)\phi(x)=0. \tag{34}$$

For higher temperatures ($k_y\rho_i > 1$) the Bessel functions can no longer be expanded and as explained earlier the terms of the order ϵ^2, such as ω_2, become less important. Neglecting ω_2 with respect to ω_1 and ignoring the density gradient in (30) and (31) we recover the starting equations for the higher frequency ion-cyclotron-like modes.[5]

III. NUMERICAL RESULTS

A. Kinetic Kelvin–Helmholtz modes

We now numerically find the eigenvalues of the general dispersion differential equation (29), which is still in the weak shear limit, first in the fluid limit to recover the fluid results for the electric field profile $E(x) = E_0\tanh(x/L)$. We then use the parameters of the simulation[7] to reproduce those elements of Table I of Pritchett and Coroniti[7] that are accessible to the weak shear limit of the theory. The differential equation (29) is solved numerically by a shooting code for the complex eigenvalues ω. We assume WKB nature of the solutions for $x \to \infty$ and impose an outgoing energy flux boundary condition. With ϕ_{WKB} and ϕ'_{WKB} specified at the boundaries for an initial eigenvalue ω_0, we use a variable stepsize integrator to obtain ϕ and ϕ' at the origin where the matching condition is examined. If the matching condition is not satisfied a new ω is assumed and the process iterates until the eigenvalue is obtained with the desired accuracy.

To recover the fluid limit we consider $\epsilon = 0.1$, $\epsilon_n = 0$, $\mu = 1837$, $\bar{V}_E = (V_E^0/v_i) = 1$, $u = k_\parallel/k_y = 0.0001$, and $\tau = 3.5$. For $k_y\rho_i = 0.02$, 0.05, and 0.08 we obtain $\gamma L/V_E^0 = 0.1369$, 0.1868, and 0.1067. These results coincide with the fluid calculations and are consistent with the normalized growth rate against the dimensionless wavenumber plot for the fluid KH instability provided in Fig. 2 of Ref. 7. Thus the fluid results are recovered from the kinetic dispersion relation for the parameter range that is fluidlike.

We now use $\tau = 1$, to match the simulation parameters.[7] Also since $\tau = 1$, $c_s = \sqrt{2}v_i$, where $c_s^2 = 2(T_e+T_i)/m_i$. For $\bar{V}_E = \sqrt{2}V_E^0/c_s = 0.764$ we find that the eigenvalues of (29) for $k_yL = 0.393$ and $\epsilon = 0.19$ and 0.38 are given by $\gamma L/V_E^0 = 0.188$ and 0.191 while the corresponding eigenvalues for $\bar{V}_E = 1.513$ are 0.184 and 0.189. Comparing these with the corresponding elements of Table I in Pritchett and Coroniti[7] we find that our theory is in agreement with the simulation results.[7] Figures 1(a) and 1(b) are the eigenfunction and the profile for the external electric field, for $\epsilon = 0.19$ and $\bar{V}_E = 0.764$. For moderate shears ($\epsilon \lesssim 0.5$) better agreement with the simulation can be expected if the assumption of

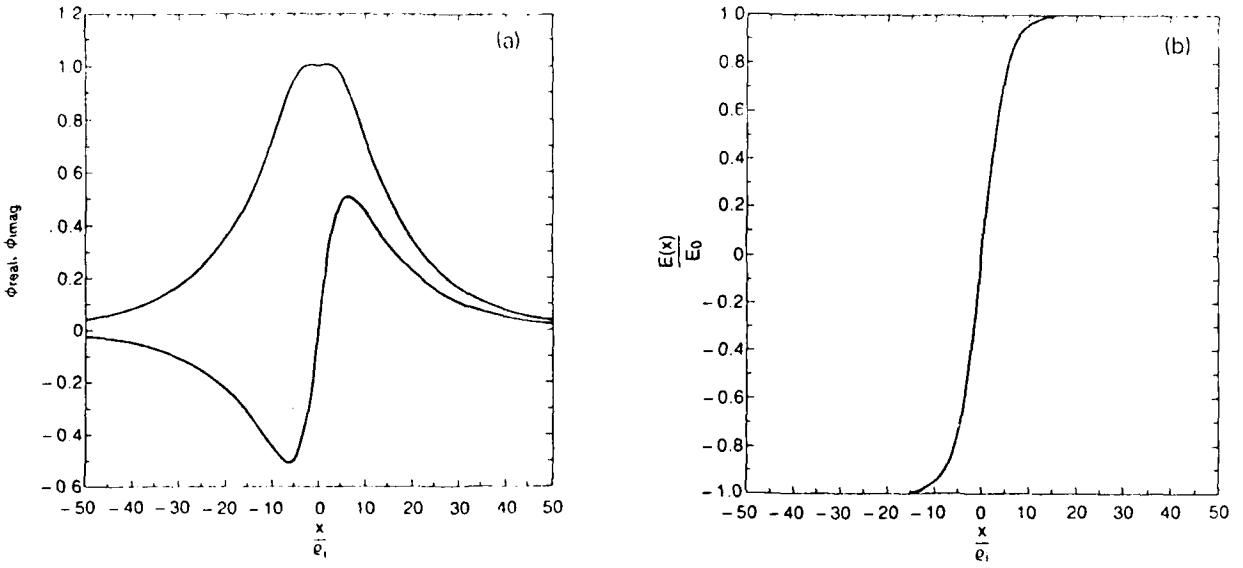

FIG. 1. Solution of the general dispersion differential equation (29) in the fluid limit. Here $\epsilon = 0.19$, $k_y\rho_i = 0.074$, $\overline{V}_E = 0.764$, $\mu = 1837$, $u = 0.0001$, and $\tau = 1$. (a) The real and imaginary parts of a typical eigenfunction. (b) The external electric field profile $E(x) = E_0 \tanh(x/L)$ for $\epsilon = 0.19$.

weak shear, i.e., $k_x' \simeq k_x$, is relaxed. This will be the subject of a future article. Higher shear values, however, are inaccessible to the theory at the present simplified differential equation level. For very high shears a dispersion relation in the form of an integral equation as provided in (17) will become necessary. Also, uncertainty in the simulation results is expected for higher shears where η differs significantly from unity (but is still positive), unless the initial loading is in accordance with the equilibrium distribution given in (4). When shear is weak and $\alpha_1 = \overline{V}_E\epsilon$ [the peak value of $V_E'(x)/\Omega$] is small, η is close to unity. For low temperatures ($\epsilon \to 0$), the equilibrium distribution function (4) can be reduced to a Maxwellian shifted in the y velocity by the magnitude of the $\mathbf{E}\times\mathbf{B}$ drift, which is approximately $V_E(x)$. Such a distribution function was used by Pritchett and Coroniti[7] for the initial loading. While acceptable for small α_1 and especially for low temperatures, this method may lead to significant relaxation of the initial state for large α_1, thereby affecting the equilibrium parameters substantially. Thus, for large α_1, the interpretation of the final simulation results[7] remains dubious.

We now study a different electric field profile, $E(x) = E_0\,\mathrm{sech}^2(x/L)$. Once again, to check the fluid limit we use $\epsilon = 0.1$, $\tau = 1$, $\mu = 1837$, and $u = 0.0001$. Figure 2 is a plot of the growth rates and the real frequency of the KH modes as obtained from Eq. (29) (solid lines) against b. The dashed lines are the fluid results provided in Drazin and Howard[9] in their Table I as sinuous mode. Good agreement can be expected for $\epsilon \ll 1$. For larger ϵ, however, the ω_2 appearing in the denominator of (32) and (33) cannot be treated as negligible. For larger ϵ, the denominator ω_2 can influence the results by enhancing the growth rates. This important temperature related effect cannot be predicted by the fluid theory including temperature, as given by Pritchett and Coroniti.[7]

A two-dimensional particle simulation[10] using an appropriate initial distribution function to study the ion-cyclotron-like modes is currently in progress. Ultimately we shall compare the KH modes with the ion-cyclotron-like modes[5] through numerical simulation as well as through theory. Thus we will use $\mu = 100$, which is being used in our simulation.[10] To study the finite gyroradius stabilization of the KH modes we plot the growth rates normalized by the ion-cyclotron frequency Ω_i against b, for various values of u in Fig. 3. We consider $\tau = 3.5$, $\epsilon = 0.43$, and a mild density gradient $\epsilon_n = 0.05$ centered around $x_{n0} = 1.33\ \rho_i$ such that $\epsilon_n = -0.05$ for $x_{n0} - \rho_i < x < x_{n0} + \rho_i$ and 0 otherwise, and as the dc electric field profile we consider $E(x) = E_0\,\mathrm{sech}^2(x/L)$ (see Fig. 4). The growth rates of the KH modes are expected to reduce because of the density gradient[11] but with the mild ϵ_n used here this decrease was not

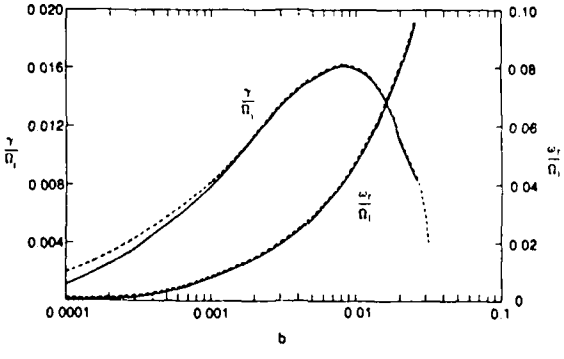

FIG. 2. The real and imaginary frequencies normalized by Ω_i for the KH instabilities for the dc electric field profile given by $E = E_0\,\mathrm{sech}^2(x/L)$ are plotted as a function of b. The solid lines are the eigenvalues of Eq. (29) while the dotted lines are the fluid results given in Ref. 9. Here $\epsilon = 0.1$, $\tau = 1$, $u = 1837$, and $u = 0.0001$.

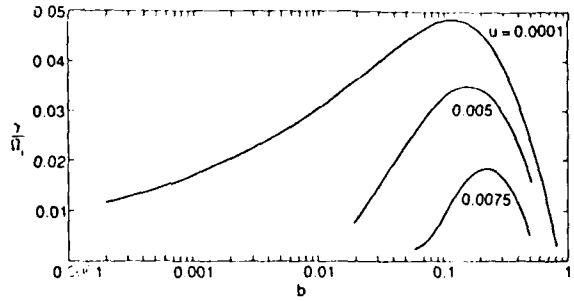

FIG. 3. A plot of the normalized growth rates of the KH modes plotted as a function of b for a number of u values. Here $\epsilon = 0.43$, $\mu = 100$, and $\tau = 3.5$.

significant. From Fig. 3 we see that for a given ϵ the growth rates peak for a particular b. The peak of the spectrum is localized for $b \sim 0.16$ ($k_y\rho_i \sim 0.4$ and $k_y L \sim 0.93$) and is maximum for transverse propagation ($u = 0.0001$). As the obliqueness u is increased, there is a sharp decrease in the peak value along with the narrowing of the spectrum. Beyond $u = 0.0075$ the growth of the KH mode is substantially reduced.

B. Ion-cyclotron-like modes

Now we consider the case where $k_y\rho_i > 1$. As explained earlier, in this domain we can no longer expand the Bessel functions, and consequently the $O(\epsilon^2)$ terms responsible for the KH modes play only a minor role. For the range in which we are now interested, where $k_y\rho_i \sim 3$, we can neglect these terms for convenience. To explain the ion-cyclotron-like modes we first resort to the piecewise continuous field profile[5] (see Fig. 5). This is an idealization of the actual field profile and we use it only to demonstrate the principles involved and to obtain a good starting eigenvalue for numerically tracking the eigenvalues for a smooth profile. For a piecewise continuous profile it is trivial to derive the nonlocal dispersion relation. Setting ω_2 and ω^* equal to zero in (30) and (31), we use (29) as the differential equation for the modes in question. In the region over which the electric field is localized (we shall refer to this region as region I) there is a Doppler shift in the frequency, i.e.,

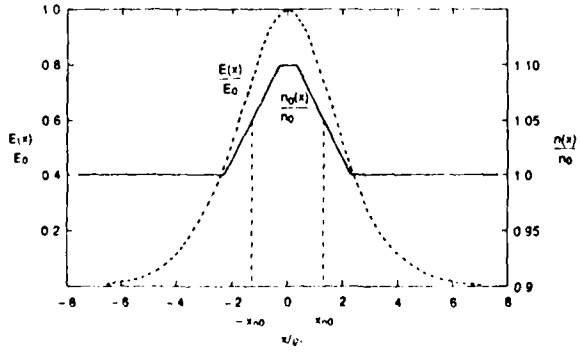

FIG. 4. The equilibrium field and density configuration used in the calculations of Fig. 3. Here $x_{s0} = 1.33\rho_i$, $\epsilon_n = -0.05$ when $x_{s0} - \rho_i < x < x_{s0} + \rho_i$ and zero otherwise.

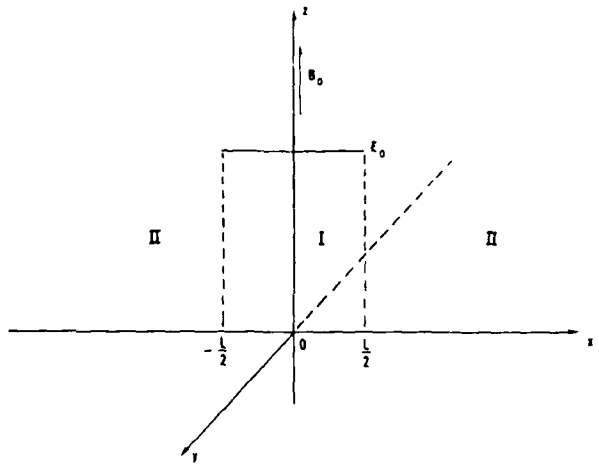

FIG. 5. A schematic representation of the piecewise continuous dc electric field profile.

$\omega \to \omega_1 = \omega - k_y V_E$, while outside this region where the electric field is nonexistent (region II) there is no shift in the frequency. This is the essential feature distinguishing the two regions. The matching condition of the logarithmic derivatives of the solutions of (29) at the boundary $x = L/2$, provides the nonlocal dispersion relation,

$$-\kappa_1 \tan(\kappa_1/2\epsilon) = i\kappa_{II}, \tag{35}$$

where $\kappa_1^2 = Q(\omega_1)/A(\omega_1)$ and κ_{II} is identical to κ_1 if ω_1 is replaced by ω. For details we refer to our earlier paper.[5] The dispersion relation was solved[5] for a wide range of parameters to find growing modes distinct from the KH modes. We first give a physical description for the origin of these modes.

The dispersion relation of the electrostatic ion Bernstein modes is[5]

$$D(\omega) = 1 - \Gamma_0(b) - \sum_{n>0} \frac{2\omega^2}{\omega^2 - n^2\Omega^2}\,\Gamma_n(b), \tag{36}$$

where $k_\parallel \sim 0$ is assumed. The energy density of these modes is

$$U \propto \omega \frac{\partial D}{\partial \omega} = \omega\left(\sum_{n>0} \frac{4\omega\Gamma_n n^2\Omega^2}{(\omega^2 - n^2\Omega^2)^2}\right) = \omega^2\sigma(\omega), \quad \sigma > 0. \tag{37}$$

Clearly, these are positive energy waves. Introduction of uniform electric field in the x direction initiates an $\mathbf{E}\times\mathbf{B}$ drift in the y direction and consequently there is a Doppler shift in the frequency, i.e., $\omega \to \omega_1 = \omega - k_y V_E$. The energy density in the presence of the Doppler shift is $U' \sim \omega\omega_1\sigma(\omega_1)$, which can be negative provided $\omega_1 < 0$. Now if we consider the localized field configuration as shown in Fig. 5, then it is clear that because of the $\mathbf{E}\times\mathbf{B}$ drift the energy density in region I becomes negative while it remains positive in region II. A nonlocal wave packet can couple these two regions so that a flow of energy from region I into region II will enable the wave to grow. Based on this simple picture we can predict some gross features of the instability. As for example, using the wave-kinetic description it is possible to obtain the energy balance condition for the system from which important scalings governing the growth rate can be predicted. The

growth of the wave in region I implies a loss of energy from that region. By conservation of energy, this must be the result of convection of energy into region II and any local energy dissipation (S_-) or free energy release (S_+) processes in region I. The rate of growth of the total energy deficit in region I is proportional to the growth rate γ, the wave energy density U_I in region I, and the volume of region I, represented here by the extent in the x direction (L) of region I times a unit area $A_\perp$ in the plane perpendicular to x. The rate of convection through $A_\perp$ is just $V_G U_{II}$, where V_G is the group velocity in the x direction and U_{II} is the wave energy density in region II. We can then write the energy balance condition as

$$\gamma U_I L A_\perp \simeq (S_+ - S_- - V_G U_{II}) A_\perp, \tag{38}$$

where S_+ and S_- represent the source and the sink in region I. The eigenvalues obtained from (35) are expected to satisfy the energy condition (38). For the situation presently under consideration we do not have any external source of free energy and since $k_\parallel \sim 0$, the natural dampings are absent. Therefore $S_+ = S_- = 0$. Now it is clear from (38) that if U_I is negative then γ can be positive and hence the growth of the wave is sustained by convection of energy into region II from region I. On the other hand if U_I is positive then the convection of energy out of region I would lead to a negative growth rate and therefore to damping of the waves. For $S_\pm = 0$, an important scaling can be predicted from (38), i.e., $\gamma/V_G \propto 1/L$, which with proper normalizations can be written as $\mathrm{Im}(k_x\rho_i) \propto \epsilon$. In Fig. 6 we plot $\mathrm{Im}(k_x\rho_i)$ against ϵ and confirm this scaling. In Fig. 6 other parameters are $\bar{V}_E = 2.9$, $\tau = 1, u = 0.0001, \mu = 1837$, and the growth rates have been maximized in b.

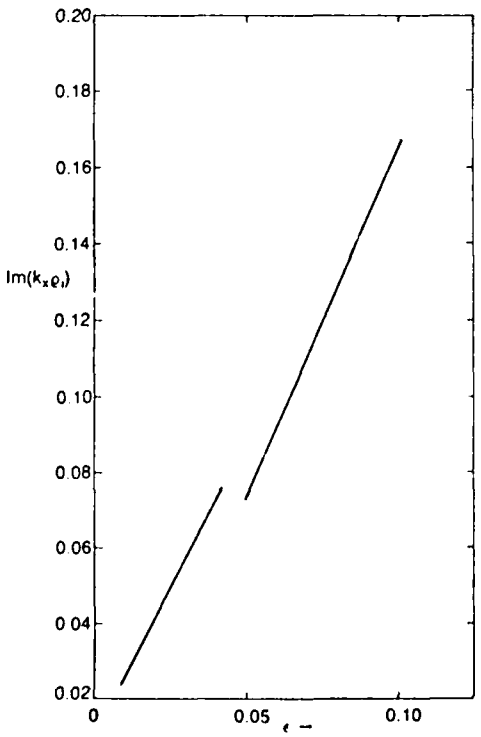

FIG. 6. A plot of $\mathrm{Im}(k_x\rho_i)$ against ϵ. The linear dependence confirms the scaling $\gamma/V_G \propto 1/L$. Here $\bar{V}_E = 2.9$, $\tau = 1$, $u = 0.0001$, and $\mu = 1837$.

We shall now study the ion-cyclotron-like modes for smooth profiles. For this we use an electric field profile given by

$$E(x) = E_0/[A \sinh^2(x/a) + 1], \tag{39}$$

where $A = 1/\sinh^2(x_0/a)$ and $x_0 = L/2$. For $a \to 0$ (39) represents a "top hat" profile that reduces to half of its peak value at $x = x_0$. As a increases the profile becomes smoother, and ultimately, when $a = x_0/\sinh^{-1}(1)$, which makes $A = 1$, expression (39) reduces to $E(x) = E_0 \operatorname{sech}^2(x/a)$. The shooting code used for the determination of the eigenvalues can operate best when the initial guess for the eigenvalue is not too far away from the actual one. Thus it becomes necessary to use (39) so that in the limit $a \to 0$ we have excellent guess values obtained analytically from the nonlocal dispersion relation (35). Starting with the eigenvalue for the $a \to 0$ case we slowly increase a to track the eigenvalues for the profiles with the desired smoothness. For $b \sim 8$ we have to retain $n = 0, \pm 1, \pm 2, \pm 3, \pm 4, \pm 5, \pm 6$ harmonics and the associated plasma dispersion functions in (29) that are evaluated numerically; thus the computations for each eigenvalue is CPU time intensive.

In Figs. 7(a)–7(d) we display the transition of the electric field profile from nearly piecewise continuous to smooth for four different values of a. Here $\epsilon = 0.3$. In Figs. 8(a)–8(d) we display the corresponding wave packets. Other parameters are $b = 8, \tau = 3.5, u = 0.011, \mu = 1837, \bar{V}_E = 0.6$, $x_{n0} = 1.66\rho_i$, and $\epsilon_n = -0.07$ if $x_{n0} - 0.9\rho_i < x < x_{n0} + 0.9\rho_i$ and zero otherwise. The growth rates did not vary much during this transition. For $a = 0.1$, 0.707, 1.41, and 1.89 the corresponding growth rates normalized by the ion-cyclotron frequency $\gamma/\Omega_i = 0.048$, 0.05, 0.037, and 0.031. There is only a 40% reduction in the growth rate from the sharp to smooth profile, and initially in going from $a + 0.1$ to $a = 0.707$ there is a slight increase in the growth rate. This is in contrast to the KH instability where the growth rates are dependent on the second derivative of the electric field and are therefore very sensitive to the scale size variation.

In Fig. 9 we provide a plot of the growth rate and the real frequency of the ion-cyclotron-like modes normalized by the ion gyrofrequency as a function of b. Here the profile in (39) is used with $a = 1.87$ and the rest of the parameters are identical to Fig. 8. We find that the instability is peaked around $k_y\rho_i \sim 3$, which for $\epsilon = 0.3$ corresponds to $k_y L \sim 10$ which is an order of magnitude larger than the corresponding value of the peak for the KH modes. Further for $u = 0.011$ used here, the KH modes are expected to be nonexistent and thus the domain for dominance for the two modes can be quite distinct. This contradicts the conclusion in Ref. 12 where a simulation based on only one set of parameters obtained from the idealized field profile[5] was used to conclude that the KH mode will always dominate the ion-cyclotron-like modes. Further the initial loading in the simulation[12] (assumed to be similar to that of Ref. 7) is improper since α_1 for the parameters used was extremely large (greater than unity), and consequently the simulation[12] showed a strong re-

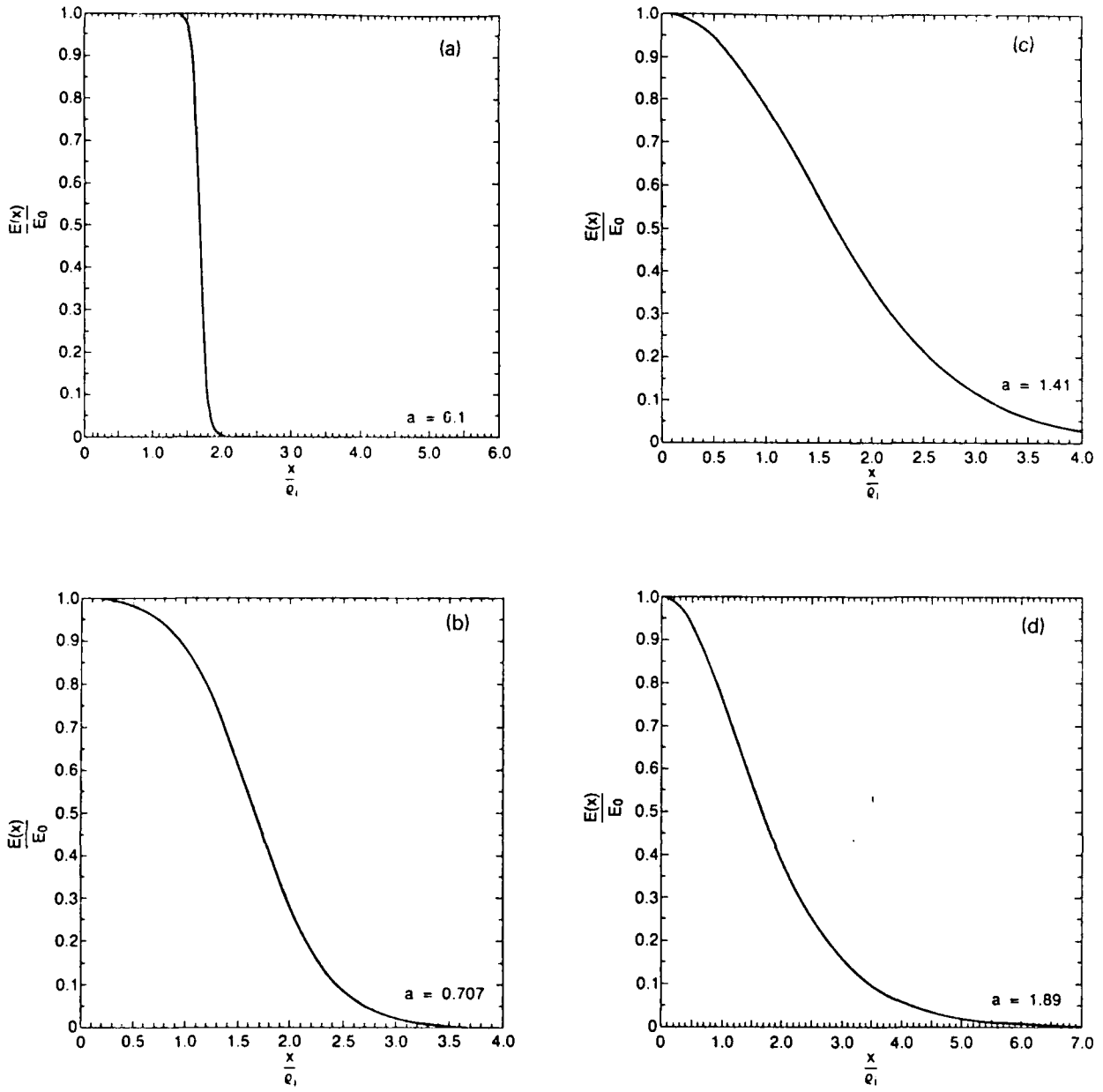

FIG. 7. The transition from a sharp to a smooth profile given in Eq. (39). Here $\epsilon = 0.3$ and (a) $a = 0.1$, (b) $a = 0.707$, (c) $a = 1.41$, and (d) $a = 1.89$.

laxation of the initial nonequilibrium velocity profile.

In Fig. 10 we use the parameters for our simulation[10] (to be discussed in a separate article), i.e., $\mu = 100$, $\tau = 3.5$, $\epsilon = 0.43$, $u = 0.038$, $\epsilon_n = -0.05$ for $x_{n0} - \rho_i < x < x_{n0} + \rho_i$ and 0 otherwise and $x_{n0} = 1.33\rho_i$ to plot the growth rate and the real frequency normalized by the ion gyrofrequency. Here for completeness we also include the ω_2 term in (29) to compute the growth rates and use exactly the same dc electric field and density profiles as were used to produce Fig. 3. The inclusion of the ω_2 term does not change the eigenvalue by much. The peak of the spectrum is around $b \sim 14$. In Fig. 3 we used the same parameters to conclude that the growth rate for the KH modes is reduced significantly for $u \geq 0.0075$ and the peak of the spectrum is around $b \sim 0.2$. Once again the domains of dominance for the KH and the ion-cyclotron-like modes are quite distinct.

Finally in Fig. 11 we provide a plot of the real and imaginary parts of the eigenfrequency ω normalized by the ion gyrofrequency Ω_i as a function of $\overline{V}_E$, the peak value of the equilibrium $\mathbf{E} \times \mathbf{B}$ drift velocity normalized by the ion thermal velocity. Here $b = 10$, $\tau = 3.5$, $\mu = 1837$, $u = 0.011$, $\epsilon = 0.3$, $x_{n0} = 1.66\rho_i$, $\epsilon_n = -0.07$ when $x_{n0} - 0.9\rho_i < x < x_{n0} + 0.9\rho_i$ and 0 otherwise. For the external electric profile we use (39) with $a = 1.87$. We see that the real frequency is almost linearly proportional to $\overline{V}_E$, which is in keeping with the experimental results of Sato *et al.*[4]

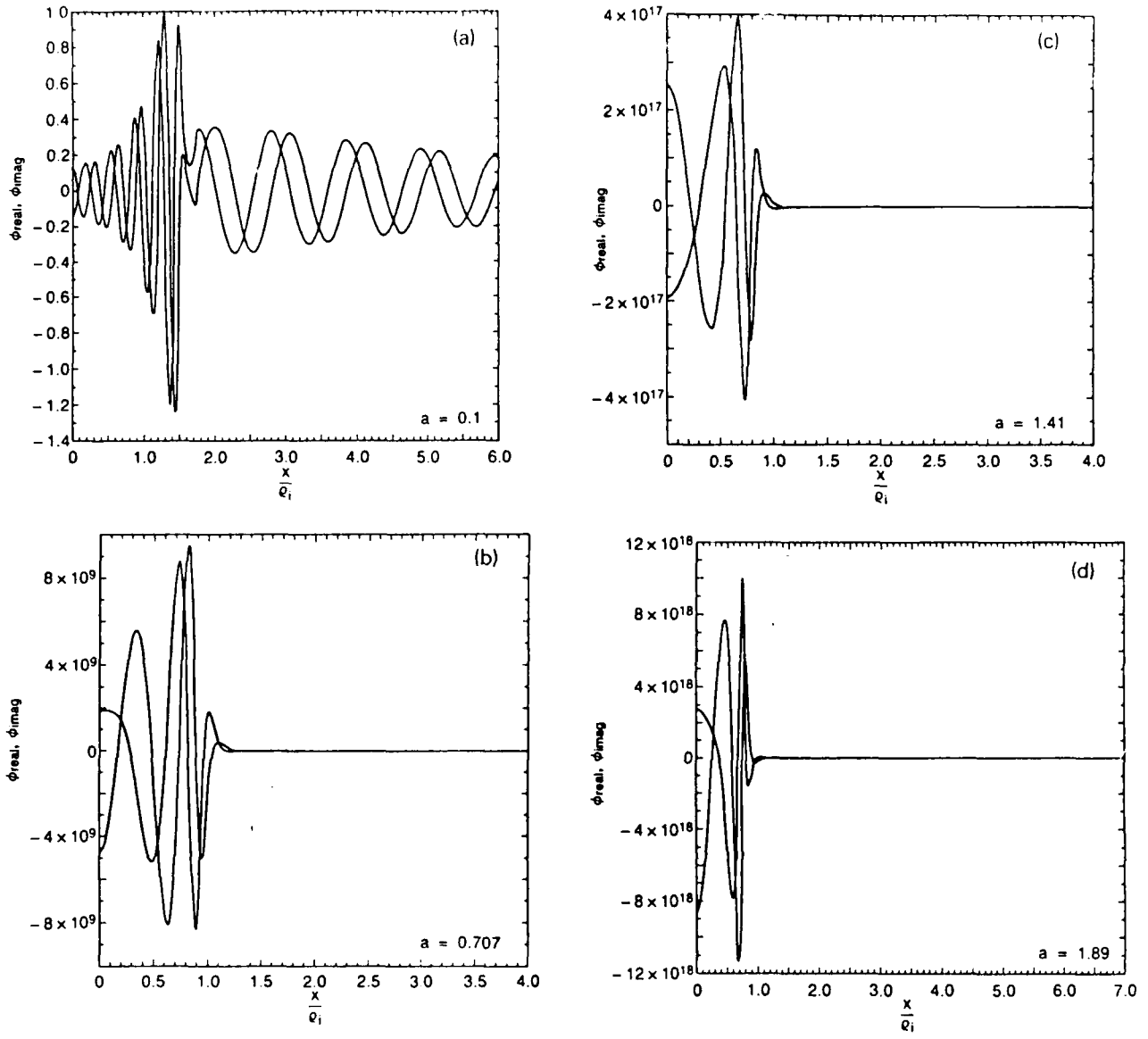

FIG. 8. The real and imaginary parts of the corresponding eigenfunctions for the profiles in Fig. 7. Here $b = 8$, $\mu = 1837$, $\overline{V}_E = 0.6$, $\tau = 3.5$, $u = 0.011$, and $\epsilon_n = -0.07$ if $x_{n0} - 0.9\rho_i < x < x_{n0} + 0.9\rho_i$ and $x_{n0} = 1.66\rho_i$. (a) $a = 0.1$, (b) $a = 0.707$, (c) $a = 1.41$, and (d) $a = 1.89$.

IV. DISCUSSION

We have provided a kinetic theory to study the electrostatic waves that can be excited in a collisionless magnetized warm plasma by a transverse velocity shear. For $k_y\rho_i \ll 1$ we recover the fluid KH modes and when $k_y\rho_i$ is increased we find that the growth rates for the KH modes are reduced and for large enough $k_y\rho_i$ the KH instability is completely damped. Further, the growth of the KH modes is severely affected by the parallel dynamics. It seems that for a collisionless plasma the KH modes can grow only for very small $k_\parallel$. As $k_y\rho_i$ becomes of order unity the expansion of the Bessel functions is no longer possible. Consequently the terms of $O(\epsilon^2)$ responsible for the KH modes diminish in importance. At this point the large $k_y\rho_i$ ion-cyclotron-like modes dominate. Further, larger $k_\parallel$ and density gradients inhibit the classical KH wave growth while both these effects favor the ion-cyclotron-like waves.

An important feature of the ion-cyclotron-like modes is the fact that the real frequency of these waves is roughly around $k_y V_E^0/2$ (see Figs. 9 and 11). This is similar to the KH waves, and therefore the two instabilities cannot be distinguished by the scaling of the real frequency with $k_y V_E$.

The linear dependence of the real frequency of the ion-cyclotron-like modes on the dc electric field was not explicitly discussed in our previous paper.[5] This could have contributed to a misunderstanding, which led Pritchett[12] to conclude that since the modes in his simulation for $\rho_i/L = 0.3$ and for $k_y\rho_i = 0.47$ and 0.94 displayed the linear dependence of the real frequency on the equilibrium flow velocity they could not be the ion-cyclotron-like modes that we have discussed. A similar misunderstanding was also dis-

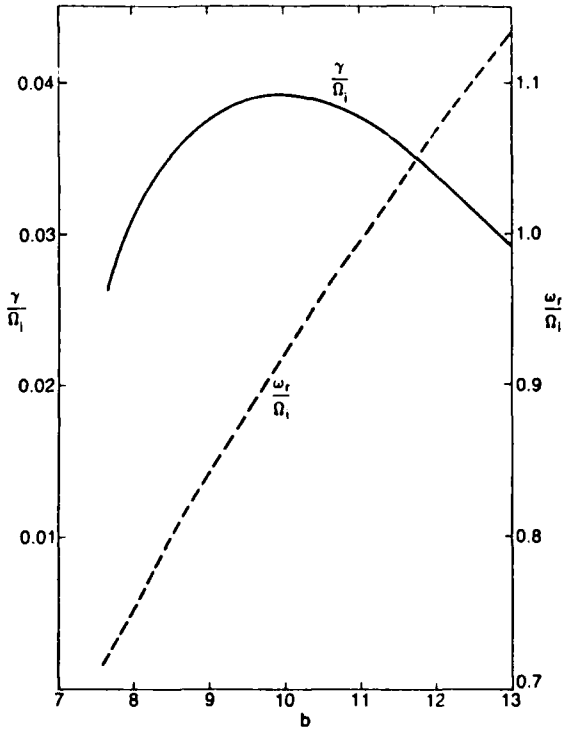

FIG. 9. A plot of the normalized real and imaginary parts of the eigenfrequency of the ion-cyclotron-like instability against b. Here $\epsilon = 0.3$, $u = 0.011$, $a = 1.87$, $\tau = 3.5$, $\overline{V}_E = 0.6$, $\mu = 1837$, $x_{n0} = 1.66\rho_i$, and $\epsilon_n = -0.07$ if $x_{n0} - 0.9\rho_i < x > x_{n0} + 0.9\rho_i$ and zero otherwise.

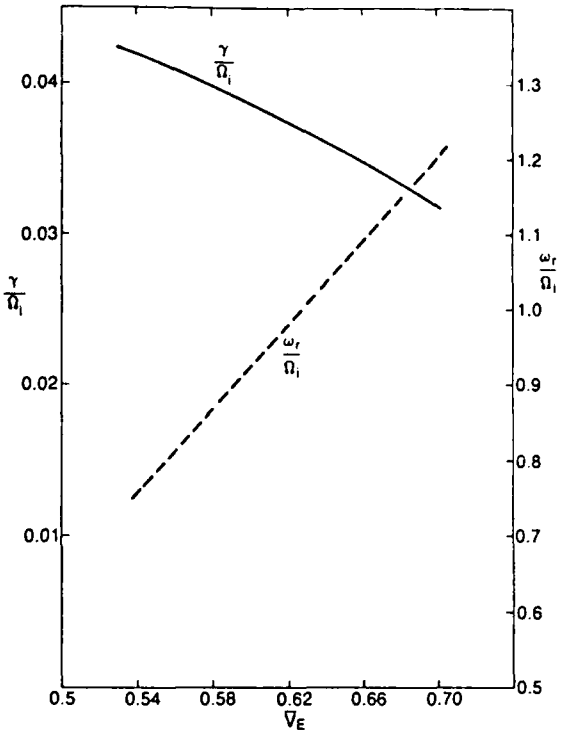

FIG. 11. The normalized real and imaginary parts of the eigenfrequency of the ion-cyclotron-like waves plotted against $\overline{V}_E$. Here $b = 10$, $\tau = 3.5$, $\mu = 1837$, $u = 0.011$, $\epsilon = 0.3$, $a = 1.87$, and $\epsilon_n = -0.07$ if $x_{n0} - 0.9\rho_i < x < x_{n0} + 0.9\rho_i$ and zero otherwise.

played by Sato *et al.*[4] in discussing their experimental results.

Since the initial electric field profile used in the simulation described in Ref. 12 was not in equilibrium, the system immediately relaxed [see Appendix A, condition (A21); here[12] $\alpha_1 = (\rho_i/a)\overline{V}_E = (2.4)3 = 7.2 \gg 1$] to what is shown in Fig. 4 of Ref. 12. This is very different from the initial profile described in their[12] Eq. (2). In fact, the initial profile is characterized by two scale lengths L and a with a peak value of about $3v_i$ while the final relaxed profile is more like a Gaussian or a $\mathrm{sech}^2(x/L)$ type characterized by only one scale length L and with a peak value of around $2v_i$. Also, as explained,[12] the spatial extent L of the electric field increased during the course of the simulation. Conservatively estimating the broadening of L by only 20%, and considering that the final profile is approximately similar to $\mathrm{sech}^2(x/L)$ with $\rho_i/L = 0.25$, then the modes at $k_y\rho_i = 0.47$ and 0.94 would correspond to $k_yL = 1.88$ and 3.76, respectively. These values will be larger if the spatial extent is broadened more than the 20% assumed. As we have shown through the analysis of the kinetic KH modes and Drazin and Howard[9] through the analysis of the fluid KH modes for shear profile of the type $\mathrm{sech}^2(x/L)$, the KH modes are strongly damped for $k_yL > 1$ and almost nonexistent beyond $k_yL \sim 2$. Thus the mode at $k_y\rho_i = 0.47$ can be the tail end of the KH spectrum but the mode at $k_y\rho_i = 0.94$ seems to be completely out of the theoretically predicted KH spectrum and the growth rate in the second mode is higher. Hence, the conclusion based on the simulations of Ref. 12 that the KH mode will always dominate over the ion-cyclotron-like modes for a configuration with a localized electric field perpendicular to an external magnetic field is at best dubious. However, we do agree with the other conclusion[12] that the idealized field profile (piecewise continuous) used earlier[5] to demonstrate the physical principles involved is not suitable for simulation

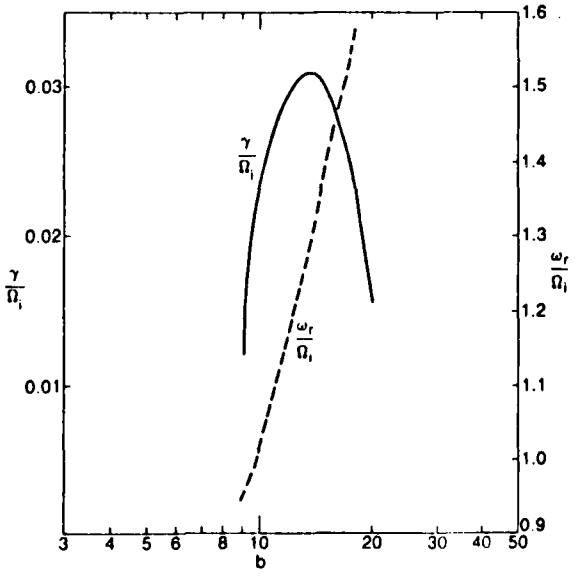

FIG. 10. A plot similar to Fig. 9. Here $u = 0.038$ and the rest of the parameters are identical to Fig. 3.

purposes and that a strong relaxation from such a profile to a smoother profile is likely. The fact that the piecewise continuous field profile is an idealization was emphasized in our earlier paper.[5] Here we have provided an equilibrium distribution (4) that, if properly loaded, should ensure a good equilibrium even for moderate shears. Since the equilibrium distribution as provided in (4), is an implicit function of ξ, the guiding center position, it is not in a convenient form for initial loading in a particle simulation. For this purpose we will express (4) in terms of the real position x. From the definition (3) for ξ we obtain

$$\xi - x = [v_y - V_E(\xi)]/\Omega. \tag{40}$$

Expanding $V_E(\xi)$ around x we can show iteratively that

$$\xi - x = [v_y - V_E(x)]/\eta(x)\Omega - [V_E''(x)/2\eta^3(x)\Omega^3][v_y - V_E(x)]^2. \tag{41}$$

Comparing (40) and (41) we find that

$$v_y - V_E(\xi) = [v_y - V_E(x)]/\eta(x) + O(\epsilon^2). \tag{42}$$

By definition $u_y = v_y - \langle v_y \rangle$ and using (42) along with the expression (11) for $\langle v_y \rangle$, we can express $u_y = [v_y - V_E(x)]/\eta(x) - O(\epsilon^2)$. Also expanding $\eta(\xi)$ around x it can be shown that $\eta(\xi) = \eta(x) + O(\epsilon)$. Using these to express w_1^2 provided in (6), in terms of x we obtain

$$w_1^2 = v_x^2 + [v_y - V_E(x)]^2/\eta(x) + O(\epsilon), \tag{43}$$

and therefore the equilibrium distribution expressed in terms of x becomes $f_0 = n_0 f_{0\perp} f_{0\parallel}$, where $f_{0\parallel} = \sqrt{\beta/2\pi}\exp(-\beta v_z^2/2)$ and

$$2\pi f_{0\perp} = \beta \exp\left[-\frac{\beta}{2}\left(v_x^2 + \frac{[v_y - V_E(x)]^2}{\eta(x)}\right)\right] \times (\sqrt{\eta(x)})^{-1}[1 + O(\epsilon)]. \tag{44}$$

It should be noted that when expressed in terms of x the η dependence in w_1^2 changes from multiplying the y component of the velocity to dividing it. The distribution given in (44) is the zeroth-order distribution function. The correction to order ϵ is given in Appendix C.

Consider the case where $\alpha_1 = V_E^0/L\Omega$, the peak value of the quantity V_E'/Ω, is much smaller than unity (weak shear). Now $\eta \to 1$ and if $O(\epsilon)$ corrections are to be ignored, then (44) becomes a Maxwellian shifted by the magnitude of the $\mathbf{E}\times\mathbf{B}$ velocity in the y direction. Such a distribution was used by Pritchett and Coroniti[7] and is acceptable for weak shears ($\alpha_1 \ll 1$) especially for low temperatures. To find the correction due to α_1, we express $1/\eta(x) = 1 - V_E'/\Omega$ along with the assumption that the temperature of the system will also be affected so that $\beta \to \beta + \delta\beta$ such that $\delta\beta \sim O(V_E'/\Omega)$. Using these approximations and $\delta\beta = \beta V_E'/2\Omega$ we can express (44) as

$$f_{0\perp} = (\beta/2\pi)\exp(-(\beta/2)\{v_x^2 + [v_y - V_E(x)]^2\}) \times (1 + [\beta V_E'(x)/4\Omega]\{[v_y - V_E(x)]^2 - v_x^2\}). \tag{45}$$

The correction term proportional to α_1 was also discussed in Ref. 7, but it was not used for the initial loading because it was expected that the system would make the necessary adjustments and that these would be small, as long as $\alpha_1 \ll 1$. Thus as long as α_1 is small the use of a shifted Maxwellian appears to be acceptable, although (45) describes a better initial distribution. For moderate shears, however, the particle loading should be in accordance with (44), otherwise strong relaxation from the initial profile[12] will be inescapable. Such strong relaxation from a nonequilibrium starting condition is invariably accompanied by substantial free energy release, which leads to a dynamic state quite different from the quiet equilibrium essential for simulation of an instability. A further improved initial distribution function with the $O(\epsilon)$ corrections included is provided in Appendix C.

It should be remarked that in most of the experiments[4] and space observations[3] there exists a magnetic field aligned current in addition to the transverse localized electric fields. In the case of an oblique double layer the magnetic field aligned current can originate from the dc electric field component in the direction of the magnetic field provided there are some collisions. As, for example, in the experiments of Alport *et al.*[4] the double layer has a component in the direction of the external magnetic field that is larger than the perpendicular component, thereby providing a large magnetic field aligned current. Further, in some recent space observations[13] ion-cyclotron-like oscillations have been reported in conjunction with simultaneous observation of a perpendicular component of a dc electric field and a magnetic field aligned current for situations where the magnitude of the magnetic field aligned current is below the threshold necessary for the excitation of the current driven ion-cyclotron instability.[14] A recent study[15] on the effect of the perpendicular electric field on the current driven ion-cyclotron instability[14] indicates that the perpendicular component of the electric field can lower the threshold for the current driven ion-cyclotron instability. The necessary condition for the current driven ion-cyclotron instability is that the parallel phase velocity $\omega/k_\parallel$ of the ion-cyclotron waves resonate with the parallel electron drift V_d, such that $(\omega - k_\parallel V_d) < 0$. For subcritical V_d, $(\omega - k_\parallel V_d) > 0$, and therefore the Landau damping cannot be inverted.[14] For simplicity again consider the idealized field profile as given in Fig. 5. The introduction of the perpendicular component of the electric field initiates an $\mathbf{E}\times\mathbf{B}$ drift and consequently there is a Doppler shift in the frequency ω, i.e., $\omega \to \omega_1 = \omega - k_y V_E$, in region I over which the electric field is localized in the perpendicular direction. Now the necessary condition for the onset of the current driven ion-cyclotron instability in region I becomes $(\omega_1 - k_\parallel V_d) < 0$, which can be satisfied even though $(\omega - k_\parallel V_d)$ remains positive. Thus the threshold value for the magnetic field aligned drift V_d necessary for the onset of the current driven ion-cyclotron instability is lowered.

For the cases where there is a magnetic field aligned drift in addition to the transverse localized electric field, the term S_+ in (38) is not zero and can roughly be estimated (using the local theory) to be proportional to $LU_1\gamma_1$, where the local growth rate in the region I, $\gamma_1 = -Q_I/Q_{R\omega}$, is evaluated at $\omega = \omega_r$. Here Q_R and Q_I are the real and the imaginary parts of the local dispersion relation identical to

the expression given in (31) with ω_2 and ω^* set equal to zero, and $Q_{R\omega}$ is the ω derivative of Q_R. In the ion rest frame the field aligned drift V_d provides an additional Doppler shift in the electron term so that Q_I is proportional to $(\omega_1 - k_\parallel V_d)$. Assuming that the field aligned current is also localized within the region I so that $Q_{R\omega} = U_I/\omega_r$ we can write the energy balance condition as

$$\gamma L A_\perp U_I \simeq -(\omega_1 - k_\parallel V_d)\omega_r L A_\perp - V_G U_{II} A_\perp. \quad (46)$$

We have neglected the ion Landau and cyclotron dampings. First consider the case where the electric field is not strong enough to make $\omega_1 < 0$ and therefore $U_I > 0$ but ω_1 is less than ω. Since $\omega_1 < \omega$ it is possible to have $(\omega_1 - k_y V_E) < 0$ when $(\omega - k_y V_E) > 0$ and hence the first term in the right-hand side of (46) provides a growth even for subcritical V_d while the convection leads to damping. Now if $\omega_1 < 0$ and consequently $U_I < 0$, the convection will lead to growth and the first term in the right-hand side will contribute to damping. However, if $k_\parallel V_d < 0$ (which can be achieved by keeping V_d constant but changing the direction of parallel propagation or vice versa) growth in region I may be expected from both the right-hand terms for $(\omega_1 - k_\parallel V_d) > 0$. This can be a likely scenario for most of the experiments and space observations involving the ion-cyclotron-like oscillations for an equilibrium that contains a dc electric field in addition to a uniform magnetic field. More details will be provided elsewhere.

V. CONCLUSIONS

Using a kinetic approach we have studied the generation mechanisms for the electrostatic waves in a magnetized warm plasma including a dc electric field perpendicular to the external magnetic field. Two distinct generation mechanisms are discussed: (i) the Kelvin–Helmholtz mechanism and (ii) the positive–negative energy wave coupling mechanism. The Kelvin–Helmholtz mechanism, first discussed about a century ago,[1] depends directly on the second derivative of the dc electric field while the other mechanism[5] depends on the inhomogeneity in the energy density of the waves. The KH instability can dominate for small $k_y\rho_i$ if the propagation is nearly perpendicular. For a collisionless plasma the KH instability is strongly damped even if $k_\parallel$ is a tiny fraction of k_y. In the theory we have shown that the terms responsible for the KH wave growth are proportional to $V_E''(x)$ and are of order ϵ^2. Only when $k_y\rho_i \ll 1$ can the Bessel functions be expanded for small argument and the order unity terms be dropped out, thereby making the order ϵ^2 terms primary. This then assures the dominance of the KH instability. When $k_y\rho_i$ is increased and is of the order of or greater than unity the Bessel functions can no longer be expanded and consequently the order ϵ^2 terms responsible for the KH waves cannot gain prominence. At this stage inhomogeneous energy density driven modes[5] dominate. Also, the dominance of the KH modes can be reduced even for small $k_y\rho_i$ if more oblique propagation (larger $k_\parallel$) is considered. Here we have also shown that the inhomogeneous energy density driven modes can tolerate larger $k_\parallel$. Thus the two modes are quite distinct and, depending on the parameter range (system size, temperature, density gradient, etc.) one or the other can dominate.

It should be pointed out that while the interpretation of the inhomogeneous energy density driven modes is quite convincing for the "top hat"-like profiles as evidenced in Fig. 6, it is not so clear cut for the smooth profiles. As the profile is made smoother, additional physics is introduced through various resonances that are now possible since ω_1 can now vary smoothly over a wide range of values as opposed to one constant value in region I and a different constant value in region II for the "top hat" profile. Geometry related effects can also play a role. It was also noted that as the smoothness of the profile was increased it was necessary to maintain a very small amount of the density gradient in the transition zone in which the electric field is reducing to zero, to preserve the growth rates. This, however, makes the model more physcial since in actual experiments (e.g., see Alport *et al.*[4]) a density gradient is present in the transition zone. It appears that the density gradient acts as a catalyst by maintaining the growth rate without much affecting the real frequency, although the exact role that the density gradient plays is yet to be fully appreciated. The important conclusion however, is the fact that besides the KH instability there is another branch that can also grow with shorter wavelengths and higher frequency in a plasma immersed in a uniform magnetic field with a nonuniform transverse electric field.

Finally we would like to point out that in the small $k_y\rho_i$ limit the integral equation can be exactly reduced to the second-order differential equation (22). Thus the second-order differential equation level of description to study the nonlocal wave dispersion properties employed in this paper is more accurate for the KH modes than the ion-cyclotron-like modes that grow for large $k_y\rho_i$. For greater accuracy the eigenvalues of the integral equation that will result by using (17) as the perturbed density must be obtained. This will be the topic of a future article.

ACKNOWLEDGMENTS

Discussions with Professor Pradip Bakshi, Dr. Y. Y. Lau, and Dr. P. L. Pritchett are gratefully acknowledged.

This work is supported by the Office of Naval Research and the National Aeronautics and Space Administration.

APPENDIX A: PARTICLE ORBITS IN A UNIFORM MAGNETIC FIELD AND A TRANSVERSE NONUNIFORM ELECTRIC FIELD

In this appendix we provide the derivation of the particle orbits to $O(\epsilon^2)$. The x and y component of the equation of motion (1) can be written as

$$\dot{v}_x = \Omega v_y - \Omega V_E(x), \quad (A1)$$

$$\dot{v}_y = -\Omega v_x, \quad (A2)$$

where $V_E(x) = -cE(x)/B_0$. Expressing (A1) in the guiding center frame ξ, and retaining terms up to $O(\epsilon^2)$ we obtain

$$\dot{v}_x = \Omega(\eta(\xi)[v_y - V_E(\xi)] - \{[v_y - V_E(\xi)]^2/2\Omega^2\}V_E''(\xi) + O(\epsilon^3)). \quad (A3)$$

We now transform (A2) and (A3) to a frame moving with a

velocity $\langle v_y \rangle$ in the y direction (i.e., $v_y \to u_y + \langle v_y \rangle$) so that

$$\dot{v}_x = \Omega(\eta(\xi)u_y + \eta(\xi)[\langle v_y \rangle - V_E(\xi)] - \{[u_y + \langle v_y \rangle - V_E(\xi)]^2/2\Omega^2\}V_E''(\xi)). \quad \text{(A4)}$$

An expression for $\langle v_y \rangle$ was given in Eq. (11) in the text. Replacing v_y by $u_y + \langle v_y \rangle$ in the right-hand side of (11), we find that $\langle v_y \rangle - V_E(\xi) = V_E''(\xi)\langle u_y^2 \rangle/2\Omega^2\eta + O(\epsilon^3)$. Substituting this in (A4) and transforming v_y to $u_y + \langle v_y \rangle$ in (A2), we obtain the equations of motion in the transformed frames to $O(\epsilon^2)$:

$$\dot{v}_x = \eta(\xi)\Omega u_y + [V_E''(\xi)/2\Omega](\langle u_y^2 \rangle - u_y^2), \quad \text{(A5)}$$

$$\dot{u}_y = -\Omega v_x. \quad \text{(A6)}$$

Note that for a linear field, $V_E'' = 0$ and (A5) and (A6) reduce to a form very similar to that of the equations of motion for zero electric field except for the factor $\eta(\xi)$ in (A5), which is a constant for a linear field. For $V_E'' = 0$ it is fairly easy to solve the equations of motion and we can obtain $u_y = A\cos\Phi$, where $\Phi = \sqrt{\eta}\Omega\tau + \bar{\Phi}$ and A is proportional to $w_\perp$. Thus for $V_E'' \neq 0$ we assume $u_y = A\cos\Phi + B\cos 2\Phi$, where $B = O(\epsilon^2)$. Differentiating (A6) once and using (A5) for $\dot{v}_x$ we obtain

$$\ddot{u}_y = -\Omega\dot{v}_x = -\eta(\xi)\Omega^2 u_y - [V_E''(\xi)/2](\langle u_y^2 \rangle - u_y^2). \quad \text{(A7)}$$

Substituting $u_y = A\cos\Phi + B\cos 2\Phi$, in the left- and the right-hand sides of (A7) we find

$$\text{lhs} = -\eta(\xi)\Omega^2 A\cos\Phi - 4\eta(\xi)\Omega^2 B\cos 2\Phi, \quad \text{(A8)}$$

$$\text{rhs} = -\eta(\xi)\Omega^2 A\cos\Phi - \{\eta(\xi)\Omega^2 B - [V_E''(\xi)A^2/4]\}\cos 2\Phi, \quad \text{(A9)}$$

where we have neglected terms smaller than $O(\epsilon^2)$. Comparing the lhs and the rhs we find that

$$B = -V_E''(\xi)A^2/12\eta(\xi)\Omega^2. \quad \text{(A10)}$$

Thus

$$u_y = A\cos\Phi - [V_E''(\xi)A^2/12\eta(\xi)\Omega^2]\cos 2\Phi, \quad \text{(A11)}$$

$$v_x = -\frac{\dot{u}_y}{\Omega} = \sqrt{\eta}A\sin\Phi - \frac{V_E''(\xi)A^2}{6\sqrt{\eta}\Omega^2}\sin 2\Phi. \quad \text{(A12)}$$

The constant A is still undetermined.

After multiplying Equation (A7) by $\dot{u}_y$ it can be written as

$$\frac{d}{dt}\left[\frac{\dot{u}_y^2}{2} + \eta(\xi)\Omega^2\frac{u_y^2}{2} - \frac{V_E''(\xi)}{2}\left(\frac{u_y^3}{3} - \langle u_y^2 \rangle u_y\right)\right] = 0. \quad \text{(A13)}$$

Using (A6) we can eliminate $\dot{u}_y$ from (A13) and define a constant $w_\perp^2$ as

$$w_\perp^2 = v_x^2 + \eta(\xi)u_y^2 - [V_E''(\xi)/\Omega^2][(u_y^3/3) - \langle u_y^2 \rangle u_y]. \quad \text{(A14)}$$

Substituting u_y and v_x from (A11) and (A12) into (A14) and retaining terms up to $O(\epsilon^2)$ it can be shown that $A = w_\perp/\sqrt{\eta}$. Thus,

$$v_x = w_\perp\sin\Phi - [V_E''(\xi)w_\perp^2/6\eta(\xi)^{3/2}\Omega^2]\sin 2\Phi, \quad \text{(A15)}$$

$$u_y = \frac{w_\perp}{\sqrt{\eta(\xi)}}\cos\Phi - [V_E''(\xi)w_\perp^2/12\eta(\xi)^2\Omega^2]\cos 2\Phi. \quad \text{(A16)}$$

With the velocities known it is a simple matter to obtain the positions,

$$x' - x = \int_t^{t'} v_x\,dx = \frac{w_\perp}{\sqrt{\eta(x)}\Omega}(\cos\Phi' - \cos\Phi) + \frac{V_E''(\xi)w_\perp^2}{12\eta(\xi)^2\Omega^3}(\cos 2\Phi' - \cos 2\Phi). \quad \text{(A17)}$$

Rewriting $\Phi' = \sqrt{\eta}\Omega t' + \bar{\Phi} = \sqrt{\eta}\Omega\tau + \Phi$, where $\tau = t' - t$ and $\Phi = \sqrt{\eta}\Omega t + \bar{\Phi}$, we obtain

$$x' - x = -[w_\perp/\sqrt{\eta(\xi)}\Omega] \times [\cos(\sqrt{\eta(\xi)}\Omega\tau + \Phi) - \cos\Phi] + [\hat{w}/12\eta(\xi)^2\Omega] \times (\cos\{2[\Phi + \sqrt{\eta(\xi)}\Omega\tau]\} - \cos 2\Phi), \quad \text{(A18)}$$

where $\hat{w} = V_E''(\xi)w_\perp^2/\Omega^2$. Similarly $y' - y$ can also be obtained. It should be noted that when $\eta \leq 0$, the orbits become unstable.

For computer simulations where a distribution of particles is under consideration we can obtain an order of magnitude restriction necessary for the stability of the orbit of a typical particle (characterized by a velocity v_t, the thermal velocity, and a displacement ρ, the gyroradius). From (A3) it is clear that as long as the first term in the right-hand side, which is of order v_t, is dominant, the form of (A3) is

$$\ddot{\chi} = -\Omega^2\eta(\xi)\chi + \text{corrections}, \quad \text{(A19)}$$

where $\chi = (\xi - x) = [v_y - V_E(\xi)]/\Omega$. Therefore the restoring force is proportional to the displacement. This ensures periodic orbits that are stable. On the other hand if the second term in the right-hand side of (A3), which is proportional to $v_t^2 V_E''(\xi)/\Omega^2$, dominates, then (A3) is of the form

$$\ddot{\chi} = \Omega[V_E''(\xi)/2]\chi^2 + \text{corrections}. \quad \text{(A20)}$$

The restoring force is now proportional to the square of the displacement. Hence the orbits are no longer periodic and therefore become unstable. Thus as long as the second term of (A3) remains smaller than the first term, i.e., $v_t^2 V_E''(\xi)/2\Omega^2 < \eta(\xi)v_t$, we can expect stable orbits for the typical particles. This restriction leads to the condition for stable orbits in a simulation:

$$\rho/R(\xi) < [2v_t\eta(\xi)/V_E(\xi)]^{1/2}, \quad \text{(A21)}$$

where $R(\xi)$ is the local radius of curvature ($= [|V_E(\xi)/V_E''(\xi)|]^{1/2}$). Simplifying (A21) by replacing the guiding center position ξ by the real position x and considering the electric field profiles of the form $V_E(x) = V_E^0 f(x/L)$, we can define $H(x)$ such that

$$H(x) = [(2v_t/V_E^0) + 2\epsilon f'(\bar{x})]^{1/2} - \epsilon[|f''(\bar{x})/f(\bar{x})|]^{1/2}, \quad \text{(A22)}$$

where $\bar{x} = x/L$ and $\epsilon = \rho/L$. In order to have stable orbits and avoid (or minimize) relaxation of the initial electric field profile used in a computer simulation, $H(x)$ should be positive for all x. If this condition is violated then the orbits will become unstable and the profile will relax until (A21) is satisfied.

APPENDIX B: THE JACOBIAN OF TRANSFORMATION IN THE VELOCITY VARIABLES

In this appendix we evaluate the Jacobian of transformation from the coordinates (x,v_x,v_y) to the coordinates $(\xi,w_\perp,\Phi)$. This Jacobian can be written as

$$J = \begin{vmatrix} \left.\frac{\partial x}{\partial \xi}\right|_{w_\perp,\Phi} & \left.\frac{\partial x}{\partial w_\perp}\right|_{\xi,\Phi} & \left.\frac{\partial x}{\partial \Phi}\right|_{w_\perp,\xi} \\ \left.\frac{\partial v_x}{\partial \xi}\right|_{w_\perp,\Phi} & \left.\frac{\partial v_x}{\partial w_\perp}\right|_{\xi,\Phi} & \left.\frac{\partial v_x}{\partial \Phi}\right|_{w_\perp,\xi} \\ \left.\frac{\partial v_y}{\partial \xi}\right|_{w_\perp,\Phi} & \left.\frac{\partial v_y}{\partial w_\perp}\right|_{\xi,\Phi} & \left.\frac{\partial v_y}{\partial \Phi}\right|_{w_\perp,\xi} \end{vmatrix}. \tag{B1}$$

Using the definition of ξ as given in Eq. (3) in the text we can evaluate the elements of the first row so that

$$J = \begin{vmatrix} \eta(\xi) - \frac{1}{\Omega}\frac{\partial v_y}{\partial \xi} & -\frac{1}{\Omega}\frac{\partial v_y}{\partial w_\perp} & -\frac{1}{\Omega}\frac{\partial v_y}{\partial \Phi} \\ \frac{\partial v_x}{\partial \xi} & \frac{\partial v_x}{\partial w_\perp} & \frac{\partial v_x}{\partial \Phi} \\ \frac{\partial v_y}{\partial \xi} & \frac{\partial v_y}{\partial w_\perp} & \frac{\partial v_y}{\partial \Phi} \end{vmatrix}, \tag{B2}$$

where we have suppressed the subscripts. Multiplying the last row by $1/\Omega$ and adding it to the first row we obtain

$$J = \begin{vmatrix} \eta(\xi) & 0 & 0 \\ \frac{\partial v_x}{\partial \xi} & \frac{\partial v_x}{\partial w_\perp} & \frac{\partial v_x}{\partial \Phi} \\ \frac{\partial v_y}{\partial \xi} & \frac{\partial v_y}{\partial w_\perp} & \frac{\partial v_y}{\partial \Phi} \end{vmatrix}. \tag{B3}$$

Thus the determinant has been considerably simplified and can be expanded as

$$J = \eta(\xi)\left(\frac{\partial v_x}{\partial w_\perp}\frac{\partial v_y}{\partial \Phi} - \frac{\partial v_x}{\partial \Phi}\frac{\partial v_y}{\partial w_\perp}\right). \tag{B4}$$

Recall that $v_y = u_y + \langle v_y \rangle$ and using the expressions for v_x and u_y from (A15) and (A16), and using equation (11) from the text for $\langle v_y \rangle$ we obtain

$$v_x = w_\perp \sin\Phi - [V_E''(\xi)w_\perp^2/6\eta(\xi)^{3/2}\Omega^2]\sin 2\Phi, \tag{B5}$$

$$v_y = \frac{w_\perp}{\sqrt{\eta(\xi)}}\cos\Phi + V_E(\xi) + \frac{V_E''(\xi)w_\perp^2}{4\eta(\xi)^2\Omega^2}\left(1 - \frac{\cos 2\Phi}{3}\right). \tag{B6}$$

The derivatives necessary in (B4) can be easily obtained, and retaining terms up to $O(\epsilon^2)$ we have

$$\frac{\partial v_x}{\partial w_\perp} = \sin\Phi - \frac{V_E''(\xi)w_\perp}{3\eta(\xi)^{3/2}\Omega^2}\sin 2\Phi, \tag{B7}$$

$$\frac{\partial v_y}{\partial \Phi} = -\frac{w_\perp}{\sqrt{\eta(\xi)}}\sin\Phi + \frac{V_E''(\xi)w_\perp^2}{6\eta(\xi)^2\Omega^2}\sin 2\Phi, \tag{B8}$$

$$\frac{\partial v_x}{\partial \Phi} = w_\perp\cos\Phi - \frac{V_E''(\xi)w_\perp^2}{3\eta(\xi)^{3/2}\Omega^2}\cos 2\Phi, \tag{B9}$$

$$\frac{\partial v_y}{\partial w_\perp} = \frac{\cos\Phi}{\sqrt{\eta(\xi)}} + \frac{V_E''(\xi)w_\perp}{2\eta(\xi)^2\Omega^2}\left(1 - \frac{\cos 2\Phi}{3}\right). \tag{B10}$$

Using (B7)–(B10) in (B4) we obtain

$$J = -\sqrt{\eta(\xi)}\,w_\perp. \tag{B11}$$

APPENDIX C: EQUILIBRIUM DISTRIBUTION WITH ORDER ϵ CORRECTION

In this appendix we provide an equilibrium distribution function suitable for initial loading for a particle simulation studying the electrostatic waves due to an equilibrium field configuration containing a uniform magnetic field and a perpendicular component of a nonuniform electric field. We shall include the corrections that are of the order ϵ but ignore the order ϵ^2 corrections for the time being. Expanding $\eta(\xi)$ around x we obtain $\eta(\xi) = \eta(x) + (\xi - x)\eta'(x) + O(\epsilon^2)$, where $\eta' = V_E''/\Omega$. Using (41) for $(\xi - x)$ we can write down

$$\eta(\xi) = \eta(x) + \{[v_y - V_E(x)/\eta(x)\Omega]\}V_E''(x)/\Omega + O(\epsilon^2). \tag{C1}$$

Also from the expression for u_y given in (A16) we find that the time average $\langle u_y^2 \rangle = w_\perp^2/2\eta(\xi)$. Expressed in terms of x,

$$\langle u_y^2 \rangle = w_\perp^2\{1 - [v_y - V_E(x)]V_E''(x)/\eta^2(x)\Omega^2\}/2\eta(x) + O(\epsilon^2).$$

Using this and (C1) in the expression for $w_\perp^2$ as provided in (6) we have

$$w_\perp^2 = v_x^2 + \frac{[v_y - V_E(x)]^2}{\eta(x)} + [v_y - V_E(x)] \times\left(\frac{v_x^2}{2} - \frac{[v_y - V_E(x)]^2}{2\eta(x)}\right)\frac{V_E''(x)}{\eta^2(x)\Omega^2} + O(\epsilon^2). \tag{C2}$$

Using (C2) in the expression for f_{01} and expanding the $O(\epsilon)$ terms we obtain

$$f_{01} = \frac{\beta}{2\pi}\exp\left[-\frac{\beta}{2}\left(v_x^2 + \frac{[v_y - V_E(x)]^2}{\eta(x)}\right)\right][\sqrt{\eta(x)}]^{-1} \times\left\{1 - [v_y - V_E(x)]\left[1 + \beta\left(\frac{v_x^2}{2} - \frac{[v_y - V_E(x)]^2}{2\eta(x)}\right)\right]\frac{V_E''(x)}{2\eta^2(x)\Omega^2} + O(\epsilon^2)\right\}. \tag{C3}$$

If the $O(\epsilon)$ term in (C3) is set equal to zero we recover (44). For even greater accuracy it is possible to obtain the $O(\epsilon^2)$ corrections also.

[1] Lord Rayleigh, *Theory of Sound* (MacMillan, London, 1896) (reprinted 1940), Vol. II, Chap. 21.

[2]A. B. Mikhailovskii, *Theory of Plasma Instabilities* (Consultants Bureau, New York, 1974), Vol. II, p. 141.
[3]F. S. Mozer, C. W. Carlson, M. K. Hudson, R. B. Torbert, B. Parady, J. Yatteau, and M. C. Kelly, Phys. Rev. Lett. **38**, 292 (1977); M. Temerin, C. Cattell, R. Lysak, M. Hudson, R. B. Torbert, F. S. Mozer, R. D. Sharp, and P. M. Kintner, J. Geophys. Res. **86**, 11278 (1981).
[4]M. Nakamura, R. Hatakeyama, and N. Sato, in *Proceedings of the Second Symposium on Plasma Double Layers and Related Topics*, Innsbruck, Austria, 1984 (Institute for Theoretical Physics, University of Innsbruck, Innsbruck, 1984), p. 224; N. Sato, M. Nakamura, and R. Hatakeyama, Phys. Rev. Lett. **57**, 1227 (1986); M. J. Alport, S. L. Cartier, and R. L. Merlino, J. Geophys. Res. **91**, 1599 (1986).
[5]G. Ganguli, Y. C. Lee, and P. Palmadesso, Phys. Fluids **28**, 761 (1985); G. Ganguli, P. Palmadesso, and Y. C. Lee, Geophys. Res. Lett. **12**, 643 (1985); G. Ganguli, Y. C. Lee, and P. Palmadesso, in *Proceedings of the Chapman Conference on Ion Acceleration*, Boston, 1985 (American Geophysical Union, Washington, DC, 1985), p. 297; P. Palmadesso, G. Ganguli, and Y. C. Lee, *ibid.*, p. 301.
[6]H. L. Berk, L. D. Pearlstein, J. D. Callen, C. W. Horton, and M. N. Rosenbluth, Phys. Rev. Lett. **22**, 876 (1969); H. L. Berk, L. D. Pearlstein, and J. G. Cordey, Phys. Fluids **15**, 891 (1972).
[7]P. L. Pritchett and F. V. Coroniti, J. Geophys. Res. **89**, 168 (1984).
[8]D. L. Jassby, Phys. Fluids **15**, 1590 (1972).
[9]P. G. Drazin and L. N. Howard, *Advances in Applied Mechanics* (Academic, New York, 1966), Vol. 7, p. 1.
[10]K. I. Nishikawa, G. Ganguli, and P. Palmadesso, Trans. Am. Geophys. Union **68**, 401 (1987).
[11]P. Satyanarayana, Y. C. Lee, and J. D. Huba, Phys. Fluids **30**, 81 (1987).
[12]P. L. Pritchett, Phys. Fluids **30**, 272 (1987).
[13]B. G. Fejer, R. W. Reed, D. T. Farley, W. E. Swartz, and M. C. Kelly, J. Geophys. Res. **89**, 187 (1984); J. Providakes, D. T. Farley, W. E. Swartz, and D. Riggin, *ibid.* **90**, 7513 (1985).
[14]W. E. Drummond and M. N. Rosenbluth, Phys. Fluids **5**, 1507 (1962).
[15]G. Ganguli and P. J. Palmadesso, Geophys. Res. Lett. **15**, 103 (1988).